# High-resolution hybrid MODIS-Landsat estimation of post-monsoon agricultural burned area in northwestern India

Tianjia Liu[1,2], Miriam E. Marlier[3], Alexandra Karambelas[4], Meha Jain[5], Sukhwinder Singh[5], Manoj K. Singh[6], Ritesh Gautam[7], and Ruth S. DeFries[3]

[1]Department of Earth and Environmental Sciences, Columbia University, NY, USA
[2]Department of Earth and Planetary Sciences, Harvard University, Cambridge, MA, USA
[3]Department of Ecology, Evolution, and Environmental Biology, Columbia University, NY, USA
[4]The Earth Institute, Columbia University, New York, NY, USA
[5]School for Environment and Sustainability, University of Michigan, Ann Arbor, MI, USA
[6]School of Engineering, University of Petroleum and Energy Studies, Dehradun, Uttarakhand, India
[7]Environmental Defense Fund, Washington DC, USA

Corresponding author: Tianjia Liu (tianjialiu@g.harvard.edu)

## Abstract

A leading source of outdoor emissions in northwestern India comes from crop residue burning after the annual monsoon (*kharif*) and winter (*rabi*) crop harvests. Agricultural burned area, from which agricultural fire emissions are derived, is difficult to quantify due to the mismatch between moderate-resolution satellite sensors and the relatively small size and short burn duration of the fires. Many previous atmospheric science studies use the Global Fire Emissions Database (GFED), which is based on the Moderate Resolution Imaging Spectroradiometer (MODIS) burned area product MCD64A1, as a bottom-up outdoor fires emissions dataset. Correction factors with MODIS active fire detections have previously attempted to account for small fires. Here we present a burned area classification algorithm that leverages more frequent MODIS surface reflectance (SR) observations (daily, 500 m) with higher spatial resolution Landsat (every 16 days, 30 m) SR observations to boost and refine MCD64A1 burned area at 30-m spatial resolution. Our hybrid MODIS and Landsat approach is based on two-tailed, quantile-based Normalized Burn Ratio (NBR) thresholds, abbreviated as ModL2T, and results in an estimated 66 ± 31% higher burned area than MCD64A1 in northwestern India during the 2003-2016 post-monsoon (October to November) burning seasons. Previous underestimation of agricultural burned area suggests that the public health impacts estimates from post-monsoon fires in this region are also conservative. We find moderate agreement between village-level fraction of ModL2T-derived burned area and surveyed farmers who burned crop residue, normalized by landholding area ($r = 0.62$, $p < 0.01$), in 2016. However, sources of error still arise from small median landholding sizes (1-3 ha), heterogeneous spatial distribution of two dominant burning practices (partial and whole field), moderate to coarse spatio-temporal satellite resolution, dark soil background, cloud and haze contamination, and possible conflation of burning with harvest. Our results suggest that fusion methods using moderate and high-resolution satellite imagery can improve agricultural fire emissions inventories by better allocating small fires spatially, thus allowing for more accurate modeling assessments of the contribution of post-monsoon agricultural fires to local and regional air quality degradation and smoke exposure in northwestern India.

# 1. Introduction

## 1.1. Agricultural residue burning in northwestern India

India is embracing agricultural mechanization to increase crop productivity and decrease labor costs in order to feed its rapidly growing population (Mehta et al. 2014). Agriculture in India is currently 40-45% mechanized, below that of the United States, Russia, Western Europe, China, and Brazil (57-95%) (Bai 2014; Mehta et al. 2014). India's population is expected to grow from 1.3 billion in 2015 to 1.7 billion by 2050 (UN 2015). This population surge demands sustainable increases in crop productivity, intensity, and yield, which in turn affects the rise of agricultural mechanization. Traditionally, farmers collect crop residue to feed livestock. However, as India mechanizes, farmers are using combine harvesters, which leave behind scattered crop residues that are labor intensive to remove manually (Vadrevu et al. 2011; Kumar et al. 2015). Consequently, 80-90% of crop residue left behind by combine harvesters is burned in field, which can severely degrade regional air quality seasonally (Sidhu and Beri 2005; Government of India 2007; Singh et al. 2008; Gupta 2012; Liu et al. 2018). More accurate burned area estimation is a critical prerequisite for improving "bottom-up" fire emissions inventories and quantifying public health impacts from air quality degradation. In this study, we target these episodic agricultural fires and build on existing methods for moderate-resolution burned area classification by integrating with complementary high-resolution satellite imagery for this region.

In northwestern India, the timing of the double cropping system particularly limits the timeframe to clear the fields of monsoon crop residue (primarily rice) during the post-monsoon (October to November). Because farmers must market rice at the earliest time possible and have limited time to sow the winter crop (primarily wheat), they often burn the crop residue (Jain et al. 2014; PRSC 2015; Ahmed et al. 2015; Gupta 2012). Thus, in spite of the restrictions on agricultural burning, farmers continue to burn crop residue due to the lack of viable, well-incentivized and cost-effective alternatives (Kumar et al. 2015; Ahmed et al. 2015; Gupta 2012).

Smoke plumes from crop residue burning blankets rural and urban areas within the Indo-Gangetic Plains (IGP), which includes Punjab and Haryana, during the post-monsoon (October to November) burning season (Figure 1). During pre-monsoon (April to May), wheat residue is burned to prepare fields for sowing the monsoon crop. In general, carbonaceous particles can be transported hundreds of kilometers in the atmosphere (Sharma et al. 2010; Kaskaoutis et al. 2014). Besides air quality degradation and public health impacts, crop residue burning reduces soil quality by depleting organic matter, major nutrients, and microbial biomass (PRSC 2015). This inhibits the productivity of the next cropping season. However, previous work using satellite fire detections and HYSPLIT atmospheric back trajectories suggests that pre-monsoon wheat residue burning is of less concern to the Delhi National Capital Region's air quality than post-monsoon rice residue burning due to different atmospheric transport patterns, higher ventilation from high boundary layer conditions, and less overall fire intensity (Liu et al. 2018). While Delhi's average post-monsoon "airshed," or the approximate region that can contribute to Delhi's air quality, encompasses most of Haryana and Punjab, the average pre-monsoon Delhi airshed shifts southward, avoiding high fire intensity areas. In addition, the influence of desert dust emissions and transport in the post-monsoon season is minimal, in comparison to the strong dust activity during pre-monsoon months (April to June), originating from the Thar desert as well as long-range transport from the Arabian Peninsula. Therefore, the burned area mapping and its quantification in this study is focused on the post-monsoon season.

### 1.2. Burned area estimation of small fires

The MODIS burned area product MCD64A1 (Giglio et al. 2009), on which the Global Fire Emissions Database, version 4 (GFEDv4) emissions are based (Giglio et al. 2013), underestimates the contribution of small fires, which has been generally accounted for with a scale factor (van der Werf et al. 2010; 2017; Randerson et al. 2012; Zhu et al. 2017). MCD64A1 is limited by its moderate spatial resolution of 500 m x 500 m. In particular, small fires < 120 ha are not well-detected (Zhu et al. 2017). Many active fires in croplands are found outside the estimated burned area extent, because the conservative detection threshold for burned area estimation often misses small fires (Randerson et al. 2012; Zhu et al. 2017). GFEDv4s, which includes a small fires boost to GFEDv4, added 79-123% in burned area to the cropland-related classes, but Randerson et al. (2012) suggest that the estimate is still conservative. Thus, higher spatial resolution satellite imagery is a necessary prerequisite to more accurately estimate burned area from small agricultural fires.

The differenced Normalized Burn Ratio (dNBR) characterizes the burn extent and severity of most fires over 2 $km^2$ in area on public lands (Key and Benson 2006). dNBR is the difference in pre-fire and post-fire NBR. NBR is defined as:

$$\mathrm{NBR} = \frac{\rho_{NIR} - \rho_{SWIR}}{\rho_{NIR} + \rho_{SWIR}} \quad (1)$$

in which $\rho_{NIR}$ and $\rho_{SWIR}$ represent the surface reflectance at near infrared and shortwave infrared wavelengths, respectively. Additionally, Picotte and Robertson (2010) find that dNBR is suitable to map many small fires within a large landscape; this is particularly relevant for agricultural fires, which are small in size and tends to cluster spatially. Indeed, global and region-specific studies have used NBR-based approaches to estimate small fires, including agricultural fires (e.g. Oliva and Schroeder 2015; McCarty et al. 2008, 2009; Randerson et al. 2012; Zhu et al. 2017; Hall et al. 2016; Wang et al. 2018). NBR is an effective indicator in mapping burn scars due to the accuracy of classification with the SWIR bands (Avery and Berlin 1992; Eva and Lambin 1998; Veraverbeke et al. 2010) and avoidance of smoke and dust susceptibility, unlike bands in the visible range of the spectrum (White et al. 1996; Roy 1999; Rogan and Yool 2001; Cocke et al. 2005).

However, burned area estimation of small agricultural fires is understudied relative to that for wildfires and remains challenging for several reasons. First, the drawdown in greenness attributed to fires can be conflated with harvest (Hall et al. 2016). The NBR of pre-harvest pixels are higher than post-harvest pixels, because the removal of biomass during harvest decreases NBR, which is dependent on vegetation greenness. Second, scene availability is limited by cloud cover and haze contamination and low temporal resolution. Because pairs of pre-fire and post-fire scenes are usually required, the acquisition timing of scenes is critical: NBR estimated from different crop stages between pre-harvest, post-harvest, and crop residue burning can affect classification. Third, unlike forest fires, which can burn continuously for days over a large area, agricultural fires are relatively small, short lasting, and vary spatially and temporally year-to-year based on the timing of harvest (Thumaty et al. 2015). Fourth, despite severe underestimation of burned area in croplands, it is also inaccurate to assume that for example, entire 500 m x 500 m MCD64A1 pixels are fully burned. Thus, simple land cover type-based correction factors (Zhu et al. 2017) may be insufficient without considering burn heterogeneity at higher spatial resolution.

Fusion MODIS-Landsat (or hybrid moderate-high resolution sensor) techniques have been developed to increase the spatial resolution of burned area mapping (e.g. Loboda et al. 2007; Boschetti et al. 2015). Many of these studies rely on statistical methods for land change detection and/or active fire "hotspot" detections as an input dataset for burn scar classification. (e.g. Loboda et al. 2007; Boschetti et al. 2015; Oliva and Schroeder 2015). In the absence of extensive ground truth data, we use MCD64A1, which integrates MODIS active fires into its land change detection-based burn scar algorithm (Giglio et al. 2009), as a reference and training dataset for establishing NBR-based thresholds and downscaling MODIS-scale burned area to Landsat resolution.

In this study, we develop a statistical two-tailed NBR algorithm using MODIS and Landsat imagery in Google Earth Engine (Gorelick et al. 2017) to rapidly classify post-monsoon (October to November) agricultural burned area in northwestern India (Punjab and Haryana) from 2003-2016. The two-tailed NBR method is a two-step classification based on thresholds for the pre-fire $NBR_{max}$ and post-fire $NBR_{min}$ composites of each post-monsoon burning season. The two thresholds are derived from the quantile-based intersection and separation of $NBR_{min}$ and $NBR_{max}$ distributions, respectively, for burned and unburned agricultural areas. We compare ModL2T-derived burned area ($BA_{ModL2T}$) to MCD64A1 and validate $BA_{ModL2T}$ with independent household survey results. In addition, we assess $BA_{ModL2T}$ in the context of two different crop residue burning practices, policy changes, mechanization (use of combine harvesters), and land fragmentation.

# 2. Data and Methods

## 2.1. Study area

The study area consists of two neighboring agricultural states, Haryana (area: 44 119 km$^2$, 2011 population: 25.4 million) and Punjab (area: 50 427 km$^2$, 2011 population: 27.7 million), in northwestern India (Figure 2; http://www.censusindia.gov.in/). Because Punjab and Haryana are situated at the heart of India's "bread basket," where most farmers predominantly follow a rice (*kharif*)-wheat (*rabi*) rotation, this region is an ideal area to perform high-resolution analysis of burned area from small fires. For our analysis, we exclude Chandigarh, an urban union territory and the capital of Punjab and Haryana.

## 2.2. Satellite data sources

The datasets used in this study are primarily derived from Landsat and MODIS (Table S1). We primarily use Google Earth Engine (GEE) to retrieve MODIS and Landsat datasets and for geospatial analysis. GEE is a cost-free, petabyte-scale cloud computing platform, which has been available since 2015 (Gorelick et al. 2017). All MODIS-derived products used in the burned area algorithm and assessments are from the Collection 6 (C6) suite. MCD64A1 C6, which replaced MODIS C5 with C6 active fires and surface reflectance products as inputs, improved on small burn scars and omission errors (Giglio et al. 2016).

*2.2.1 Double crop-fire cycle*

We first characterize the seasonal and diurnal temporal distributions of fires in northwestern India. Following Vadrevu et al. (2011), we use the 1-km combined MODIS/Terra and Aqua active fire counts (MCD14ML) to show the average annual distribution of fires from 2003-2016. We also complement the fires with median NBR, estimated from MODIS MOD09A1 8-day composite surface reflectance (SR) to show variations in greenness in the rice-wheat double cropping system of northwestern India. Giglio (2007) estimates an afternoon peak fire energy of 4:30 pm in central India based on Visible and Infrared Scanner (VIRS) active fires. Central India primarily consists of croplands with major *kharif* rice-growing areas (Mahajan et al. 2017). Vadrevu et al. (2011) use the MODIS Terra/Aqua Fire Radiative Power (FRP) ratio to estimate a post-monsoon peak fire energy of ~2:12 pm in Punjab. GFEDv4s also estimates the 3-hourly diurnal cycle of fire emissions based on active fire observations from the Geostationary Operational Environmental Satellite (GOES) Wildfire Automated Biomass Burning Algorithm (WFABBA) (Mu et al. 2011).

### 2.3. The ModL2T algorithm for high-resolution burned area classification

*2.3.1 Burned area estimation*

Previous studies on high-resolution agricultural burned area estimation in northwestern India are generally constrained to 1-2 years of study (e.g. PRSC 2015; Yadav et al., 2014a; 2014b). Here we use GEE to expand the study time period to 14 years and estimate post-monsoon agricultural burned area from 2003-2016. The post-monsoon burning season is defined as October 1 to November 30. Figure 3 describes the workflow for the ModL2T algorithm in GEE. The ModL2T algorithm can be summarized as follows: (1) pre-process individual scenes; (2) composite cloud-free scenes in pre-fire and post-fire collections; (3) define two-tailed thresholds based on the quantile intersection of NBR in burned and unburned agricultural areas; (4) separately derive MODIS and Landsat burned area; (5) merge Landsat and MODIS classifications and apply agricultural mask.

Our method is primarily based on the MODIS MCD64A1 global burn mapping algorithm and GFEDv4s small fires boost approach (Giglio et al. 2009; Randerson et al. 2012). We integrate moderate and high-resolution classification of seasonal fires in one region and land cover type: croplands in northwestern India. MCD64A1 uses dynamic NBR-based thresholds, based on 1-km MODIS active fire detections for selecting burned and unburned training pixels, and is validated with Landsat-derived burned area maps (Giglio et al. 2009). Here we use MCD64A1 as a training dataset due to the lack of extensive ground data and viability of visual interpretation for the 14-year duration of the study period and large extent of the study region. MODIS-scale training data provides an endmember of larger clusters of small burn scars from which we can obtain the spectral signature and apply to Landsat at higher resolution. A high fraction of fields within a MODIS or Landsat pixel may collectively burn crop residues within several days, which effectively increases probability of burned area classification from a pre-burn to post-burn spectral difference standpoint. Because the Landsat pixel area (30 m) is more than two orders of magnitude smaller than the MODIS pixel area (500 m), the fraction of burned fields per pixel required to cross the burned area classification threshold is lower for Landsat. ModL2T thus adapts the MCD64A1 algorithm for use with Landsat imagery in GEE. We improve on "baseline" MCD64A1 burned area estimation with a Landsat-driven small fire boost – similar to the Randerson et al. (2012) GFEDv4s approach of using active fires to boost

MCD64A1 – that increases the spatial resolution (500 m to 30 m) but decreases the temporal resolution (daily to bimonthly) of MCD64A1.

We use the near infrared and shortwave infrared SR bands from MODIS/Terra (MOD09A1) and Landsat 5 (TM), 7 (ETM+), and 8 (OLI/TIRS) SR products to estimate NBR (Tables S1, S2). We use MODIS/Terra daily surface reflectance rather than that of Aqua, because the local daytime overpass time of the MODIS/Terra (10:30 am) – that of the MODIS/Aqua is 1:30 pm – is comparable with that of Landsat (10:00 am ± 15 minutes). MOD09A1 is a gridded Level-3, validated stage 2 product that selects the best quality pixel over every 8-day period based on several criteria: cloud cover, observation coverage, low-view angle, and aerosol loading (Vermote and Kotchenova 2008).

While available MODIS/Terra and Landsat 7 scenes cover the study area for all years from 2003-2016, Landsat 5 scenes only cover 2003-2010 and Landsat 8 scenes from 2013-2016. We do not gap-fill Landsat 7 scan line errors and account for such pixels as "no data." We only consider pixels as marked "clear" by quality flags. Cloud or haze-contaminated pixels are additionally filtered using the normalized difference of the SWIR and Red bands, based on Xiang et al. (2013). Visible bands are more sensitive to cloud contamination than SWIR bands; pixels where the SWIR SR exceeds Red SR are retained:

$$\frac{\rho_{SWIR} - \rho_{Red}}{\rho_{SWIR} + \rho_{Red}} > 0 \qquad (2)$$

Burned area from MODIS and Landsat is separately derived from NBR due to possible errors from differences in spatial resolution (500 m versus 30 m). Based on Vadrevu et al. (2011), we leverage knowledge of the timing of the *kharif* rice crop and fire activity patterns in Punjab and Haryana to define time brackets for pre-fire and post-fire image collections. MODIS and Landsat $NBR_{max}$ (maximum NBR composite from pre-fire image collection: August 1 to September 30) and $NBR_{min}$ (minimum NBR composite from post-fire image collection: October 1 to November 30) images serve as the two classification criteria of burned area on the basis that agricultural burned area generally have high $NBR_{max}$ (pre-fire) and low $NBR_{min}$ (post-fire). For croplands, the drawdown in greenness from burning can be conflated with harvest, so the drop in NBR is not as abrupt as wildfires. However, burned vegetation and ash exhibit a more negative difference between NIR and SWIR SR (or lower NBR) than bare soil and stubble (Lewis et al. 2011; Pleniou and Koutsias 2013; Wang et al. 2018). Thus, we expect $NBR_{min}$ for burned fields to be lower than for unburned (fallow) fields.

The $NBR_{max}$ and $NBR_{min}$ thresholds are determined from the quantile-based separation of $NBR_{max}$ and $NBR_{min}$ distributions of burned and unburned agricultural areas, based on MODIS MCD64A1 burned area (500 m) and the "cultivated land" class from the GlobeLand30 land cover map for 2010 (Table S1). GlobeLand30 is a global 30-m, 10-class land cover map derived from > 20,000 Landsat and Chinese HJ-1 satellite images (Chen et al. 2014; Chen et al. 2017; globallandcover.com). According to the University of Maryland MODIS-derived land cover classification (MCD12Q1, C6) from 2003-2016, cropland area not varies minimally (coefficient of variation: 0.3%) from year to year in the study region. We define the two-tailed classification thresholds as the average composite MODIS NBR ($NBR_{min}$ or $NBR_{max}$) at the quantile-based intersection of the $\tau$ percentile of MCD64A1-burned NBR and 1- $\tau$ percentile of unburned NBR:

$$T = \frac{1}{2}\left[Q_{f(X)}(\tau) + Q_{f(Y)}(1-\tau)\right] \quad (3)$$

where $T$ is the $NBR_{max}$ or $NBR_{min}$ threshold, $Q(\tau)$ is the quantile function at $\tau$ percentile of the probability density function, $f$, of the distribution of $NBR_{min}$ or $NBR_{max}$ at burned ($X$) and unburned ($Y$) agricultural areas. This approach attempts to balance omission and commission errors. $T_{max}$ ranges from 0.635 to 0.706, and $T_{min}$ ranges from -0.057 to -0.014. Figure 4 shows an example of derived $T_{min}$ and $T_{max}$ for 2016. The quantile-based thresholds are generally located around $\tau$ = 0.71 for $T_{min}$ and $\tau$ = 0.29 for $T_{max}$. This indicates that 71% unburned and burned agricultural areas are on average separated for each threshold. We also test the sensitivity of $T_{min}$ and $T_{max}$ using VIIRS active fire geolocations, over 2012-2016, as an independent training dataset: we find that VIIRS-trained $T_{min}$ and $T_{max}$ on average differ by +0.01 and -0.04, respectively, from MCD64A1-trained NBR thresholds, and achieve on average 61% and 65% of separability for $NBR_{min}$ and $NBR_{max}$ distributions, respectively. These small differences suggest that despite its coarser resolution, MCD64A1 can train $T_{min}$ and $T_{max}$ as well as VIIRS due to saturation in separability.

We use the MODIS-derived thresholds $T_{max}$ and $T_{min}$ on Landsat $NBR_{max}$ and $NBR_{min}$, because MCD64A1 (500 m) is relatively coarse compared to Landsat resolution. Sensor-specific differences in spectral band wavelengths and the lack of Landsat availability can also introduce bias (Table S2, Figure S1). Thus, before deriving burned area from Landsat imagery, we correct for bias in Landsat NBR composites by adding the yearly regionally-averaged differences in MODIS and resampled Landsat NBR to Landsat NBR for all Landsat platforms. The compensation for Landsat $NBR_{max}$ ranges from 0.012 to 0.114, and that for $NBR_{min}$ ranges from -0.073 to 0.012. In this step, we merge the MODIS-derived burned area with the MCD64A1 product itself to minimize omission error generated by differences in the MCD64A1 and ModL2T algorithms.

Next, to merge the separately derived MODIS and Landsat classified burned area, we "carve" out moderate-resolution MODIS burned pixels with high-resolution Landsat burned pixels (Figure S1). That is, we are more confident in Landsat than MODIS to distinguish between individual burned and unburned fields. Because more individual landholdings are mapped together due to its coarser spatial resolution, MODIS tends to overestimate (underestimate) burned area for larger (smaller) clusters of burnt fields. However, due to Landsat's coarse temporal resolution, we are not confident in Landsat to accurately capture the highest $NBR_{max}$ and lowest $NBR_{min}$ when its usable data availability is temporally-sparse and/or biased. Thus, we first create a criterion to mask such areas. After resampling to MODIS resolution, Landsat $NBR_{min}$ and $NBR_{max}$ that deviate more than ± 0.1 from MODIS $NBR_{min}$ or $NBR_{max}$ are masked. With this criterion, Landsat $NBR_{min}$ and $NBR_{max}$ must approximately agree with those of MODIS for the ~238 Landsat burned and unburned pixels to take precedent and replace a MODIS pixel. The NBR absolute difference threshold of 0.1 allows for some variance for composites of best quality Landsat pixels from different acquisition dates and sensor-specific differences in spectral band wavelengths (Table S2). While 0.1 is an arbitrary selection, a large departure of Landsat from MODIS NBR indicates that pixels of available Landsat scenes are generally cloudy and/or do not capture scenes near peak monsoon growing season ($NBR_{max}$) and/or in the post-burning ($NBR_{min}$) period when the burn scar is still visible. Furthermore, it may be the case that there are some Landsat observations in the two-month windows of the pre-fire and post-fire collections, but the acquisition dates of "best quality" Landsat pixels may not be close to that for MODIS pixels. In the last step, we apply an agricultural mask based on GlobeLand30 land cover. The final ModL2T-derived burned area (BA$_{ModL2T}$) is an estimate of the total post-monsoon agricultural burned area at the Landsat 30-m resolution.

We also assign confidence scores to BA$_{ModL2T}$ on a pixel-by-pixel basis by designating different categorical values to burned area derived from MCD64A1, Landsat-only ModL2T, and MODIS (MOD09A1)-only ModL2T. We are most confident in MCD64A1 and least confident in MODIS-only ModL2T, so we assign BA$_{MCD64A1}$ a value of 3, Landsat-only BA$_{ModL2T}$ a value of 2, and MODIS-only BA$_{ModL2T}$ a value of 1. Adding these burned area layers together yields a confidence scale from 1 (low) to 6 (high) (Table S4).

*2.3.2. MCD64A1-based geographical accuracy assessment*

We use MCD64A1 as the reference dataset in a geographic accuracy assessment of the two-tailed threshold burned area classification algorithm. Here, we compare MCD64A1 with MODIS (MOD09A1)-only BA$_{ModL2T}$ in order to evaluate the burned area classification algorithms on a pixel-by-pixel basis at the MODIS 500-m resolution. We estimate Cohen's kappa coefficient ($\kappa$), which evaluates the agreement between the reference and test classification after random chance is removed (Cohen 1960).

*2.3.3. Validation using household survey results*

We validate BA$_{ModL2T}$ by using a 2016 survey on farm management practices across the IGP. The 2016 survey data asks participants about burning crop residue in the post-monsoon (Did you burn crop residue before planting wheat?) and includes GPS coordinates. Because the survey responses inherently distinguish between burned versus unburned fields, this validation addresses the conflation of burning versus harvest. We use 1111 responses from farmers in 30 Punjab and 32 Haryana villages. However, the GPS coordinates are located not in-field, so we cannot match responses to individual fields. We therefore group responses by village name and match mean GPS coordinates with an accuracy < 10 m to the village shapefiles. On average, 18 ± 5 households were surveyed per village. We normalize the % households that burn crop residue with landholding area by village in post-monsoon 2016. For comparison, we estimate the % BA$_{ModL2T}$ of total village cultivated area based on GlobeLand30. Due to these normalized approximations spurred by data limitations, the two metrics of % burning per village are not comparable in absolute terms.

*2.3.4. Further assessments of ModL2T-derived burned area*

In lieu of a single "ground truth" validation, we further assess BA$_{ModL2T}$ with simple checks using: (1) pixel-level (active fire locations), (2) district-level (previous burned area estimates) and (3) region-level (satellite aerosol optical depth, AOD). We consider $p < 0.01$ to be statistically significant.

**Assessment 1 (VIIRS active fire locations):** The GFEDv4s small fires boost approach uses the ratio of dNBR at active fire locations outside and inside burned areas (Randerson et al. 2012; van der Werf et al. 2017). In line with this approach based on the co-location of fires and burned area, we use higher spatial resolution (375 m) Visible Infrared Imaging Radiometer Suite (VIIRS) active fire geolocations (VNP14IMGML, Collection 1) over October and November in 2012-2016 to assess omission errors. We consider daytime VIIRS active fire detections classified as "presumed vegetation fire" (Schroeder and Giglio, 2018). This assessment is based on the fraction of VIIRS active fires co-located within the classified burned area; a higher fraction indicates a lower omission error. $BA_{ModL2T}$ and $BA_{MCD64A1}$ are first resampled to a coarser 1-km resolution to approximately account for off-nadir MODIS and VIIRS pixel area. A 1-km pixel with one of more $BA_{ModL2T}$ and $BA_{MCD64A1}$ is considered burned.

**Assessment 2 (previous burned area estimates):** We compare post-monsoon district-level $BA_{ModL2T}$ to that of PRSC (2015) and Yadav et al. (2014a; 2014b). PRSC (2015) estimated district-level burned area from post-monsoon burning in Punjab in 2014 and 2015 by performing classification on multi-date Normalized Difference Vegetation Index (NDVI) from high-resolution multi-sensor (Landsat 8, AWiFS and LISS-3) satellite imagery from October 15 to November 15. Yadav et al. (2014a; 2014b) used the Iterative Self-Organizing Data Analysis (ISODATA) clustering classifier in multi-date unsupervised classification of AWiFS satellite-derived NDVI images to estimate agricultural burned area in ten districts (Ambala, Faridabad, Jind, Kaithal, Karnal, Kurukshetra, Panipat, Sirsa, Sonipat, and Yamunanagar) in northern Haryana in 2013 and three districts (Kaithal, Karnal and Kurukshetra) in 2010, respectively. PRSC (2015) and Yadav et al. (2014a; 2014b) validated district-level burned area classifications using ground truth GPS points and/or field photographs.

**Assessment 3 (MODIS AOD):** Aerosol optical depth (AOD) represents the column-integrated aerosol loading and measures the extinction of solar radiation. High AOD values represent hazy conditions and generally poor air quality. We use Level-2 AOD product from MODIS/Terra, operationally available at 3-km and 10-km pixel resolution, to assess detrended correlation with $BA_{ModL2T}$ (Table S1). Mid-visible AOD retrievals at 0.55 μm are used in this study. The Level-2 AOD retrievals are available on a daily basis, which were then uniformly gridded to produce a per-pixel AOD mean spatial distribution at 3 x 3 km and 10 x 10 km grid cells, for Punjab and Haryana. The data were then averaged for each post-monsoon period from 2003-2016. For the 10-km AOD retrieval, we use the combined Dark-Target (DT) and Deep-Blue (DB) product, which merges aerosol retrievals over both dark vegetated and bright reflecting regions (e.g. arid/desert areas except snow surface) (Singh et al. 2017). In terms of accuracy of the 10-km product, the expected error envelope is reported to be $\pm (0.05 + 0.15\tau)$ over land (Levy et al. 2013) for DT retrievals and $\pm (0.03 + 0.2\tau)$ for DB retrievals (Sayer et al. 2013), where $\tau$ represents AOD. This combined DT/DB product uses NDVI climatology for differentiating between dark and bright land areas. In this study, we use the best-quality retrievals of the combined DT/DB AOD data (for only quality flag = 3 retrievals). Additionally, the 3-km AOD retrievals are also used to analyze spatial distribution of aerosol loading at a higher resolution and study relationship with burned area. The 3-km AOD data are based on DT retrievals, limited to vegetated pixels, which cover the majority of Punjab and Haryana. The uncertainty of the 3-km AOD retrieval is reported as $\pm (0.05 + 0.15\tau)$ (Munchak et al. 2013), where $\tau$ represents AOD.

## 2.4 Landholdings and combine harvesters

We consider ancillary data in landholding size and combine harvester use to assess trends in farm fragmentation and mechanization. The Agricultural Census division of Indian Department of Agriculture, Cooperation, and Farmers Welfare conducts the Agricultural Census in India (http://agcensus.nic.in/) and provides two online databases: Agricultural Census and Input Survey. The online database of the Agricultural Census, which is based on census and input sample survey, contains quinquennial data regarding the number, average size and area of landholdings by country, state, district and tehsil (sub-district) and by social group (caste, tribe) and gender from 1995-96 to 2010-11 (http://agcensus.dacnet.nic.in/). The Input Survey is another online database with quinquennial data of detailed information about agricultural implements and machinery, including total combine harvesters by landholding size, from 1996-97 to 2011-12 (http://inputsurvey.dacnet.nic.in/). The 2016 household survey also asks participants about harvest methods (How do you harvest your rice crop?). The possible response choices are: (1) fully mechanical (e.g. combine harvester), (2) partially mechanical (e.g. thresher), (3) manually, (4) both manual and mechanical, (5) other and (6) never harvested rice. We use all responses from farmers in Punjab and Haryana to assess the relationship between combine harvester use and rice residue burning before sowing wheat.

### 2.5. Methods of crop residue burning

In a field visit, Kumar et al. (2015) identified two dominant crop residue burning practices in Punjab: (1) whole field burning and (2) partial burning (small stalks). We use Google Earth's collection of sub-meter to meter fine-resolution historical imagery (DigitalGlobe and CNES/Airbus) to qualitatively characterize crop residue burning practices (e.g. whole field, partial field burning) at the resolution of individual fields in Punjab and Haryana. We discuss the differences in scarring from and spatial distribution of the two dominant burning practices. Publicly available images are limited, often acquired outside the post-monsoon period; most scenes assessed were acquired in 2014-2016.

## 3. Results

### 3.1. Spatio-temporal distributions in fire activity

Figure 5a shows the average annual timing of the bimodal fire activity and the double-crop system in northwestern India. Whereas high NBR represents high vegetation cover (peak greenness) during the monsoon and winter crop growing seasons, low NBR represents low vegetation cover (bare soil, burn scars) after harvest and crop residue burning. MCD64A1 burn frequency shows repeated post-monsoon fire activity from 2003-2016, particularly in southern-central Punjab (Figure 5b), where fires tend to occur later in the fire season than in parts of northern Punjab (Figure 5c). In addition, Aqua (1:30 pm local time) averages 645 ± 289 % higher in fire counts than Terra (10:30 am local time) during the 2003-2016 post-monsoon burning seasons, which is consistent with the afternoon peak fire energy (4:30 pm local time) estimated by Giglio (2007). Estimates from 3-hourly GFEDv4s, based on Mu et al. (2011), and Vadrevu et al. (2011) point to an earlier (~2:12 pm local time) post-monsoon peak fire energy in Punjab (Figure S3). However, Vadrevu et al. (2011) is limited by MODIS Terra/Aqua overpass times, and Mu et al. (2011) use land cover type matching to broadly attribute normalized fire diurnal cycles globally based on GEOS observations in North and South America.

### 3.2. ModL2T-derived burned area

#### *3.2.1. Comparison to MCD641 burned area estimates*

The strength of agreement (Cohen's κ) between $BA_{MCD64A1}$ and MODIS-only $BA_{ModL2T}$ is consistent and ranges from 0.4-0.53 (moderate) (Landis and Koch 1977). Overall accuracy ranges from 82-89%. ModL2T averages 66 ± 31% higher post-monsoon burned area than

MCD64A1 in Punjab and Haryana from 2003-2016 (Figure 6, Table S3). We estimate 49-72% of $BA_{ModL2T}$ with good confidence (score ≥ 3) (Figure S2). In terms of $BA_{ModL2T}$ in excess of $BA_{MCD64A1}$, Landsat-only $BA_{ModL2T}$ (33%, score = 2) generally dominates MODIS-only $BA_{ModL2T}$ (6%, score = 1). $BA_{ModL2T}$ in 2003-07 and 2011-12 may be less accurate as a result of relatively low availability of usable and cloud-free data for MODIS and/or Landsat (Figures S1, S2). Proportionally, $BA_{MCD64A1}$ in Haryana constitutes a smaller fraction (14 ± 3%) of total burned area in the study region than $BA_{ModL2T}$ (24 ± 3%). This indicates that the ModL2T increase in burned area over MCD64A1 is partly driven by its additional burn scar detections in Haryana.

### *3.2.2. Validation with 2016 household survey*

Figure 7a shows the spatial comparison between $BA_{MCD64A1}$ and MODIS-only $BA_{ModL2T}$ in 2016. The overall accuracy is 84% with moderate agreement ($\kappa = 0.53$) (Table 1). Disagreements between $BA_{MCD64A1}$ and MODIS-only $BA_{ModL2T}$ mainly lie in central Haryana and northern Punjab. We validate $BA_{ModL2T}$ with independent household survey results from 2016. We compare post-monsoon village-level survey crop residue burning rates, normalized by landholding size, with $BA_{ModL2T}$ expressed as a fraction of cropland area. The village-level fraction of surveyed households that burn crop residue is moderately correlated with fractional $BA_{ModL2T}$ ($r = 0.62$, $p < 0.01$) (Figure 8a). In contrast, $BA_{MCD64A1}$ achieves a weaker correlation of $r = 0.54$ ($p < 0.01$) and tends to cluster at fractions burned of 0 or 1, likely due to its moderate spatial resolution (Figure 8b). $BA_{MCD64A1}$ and $BA_{ModL2T}$ explain 28% and 37% of variability (adjusted $R^2$) in survey burn rates, respectively, indicating that $BA_{ModL2T}$ is better able to capture variability in the "ground truth" burn rates.

### *3.2.3. Additional assessments of $BA_{ModL2T}$ and $BA_{MCD64A1}$*

We first assess omission error based on the fraction of VIIRS active fire detections co-located with $BA_{MCD64A1}$ and $BA_{ModL2T}$, during the 2012-2016 post-monsoon burning seasons. With a higher spatial resolution (375 m) than MODIS/Terra and Aqua (1 km), VIIRS is able to more consistently detect smaller and cooler fires (Figure S4). We find that $BA_{ModL2T}$ and $BA_{MCD64A1}$, resampled to 1 km, are co-located with 95-100% (0-5% omission error) and 69-76% (24-31% omission error), respectively, of VIIRS-detected active fires within cropland areas (Table S5). The maximum commission error is slightly higher for $BA_{ModL2T}$ (18-23%) than $BA_{MCD64A1}$ (13-17%) but may reflect undetected active fires outside VIIRS overpasses or obscured by thick haze or clouds. In particular, $BA_{MCD64A1}$ is often unable to detect active fire hotspots in regions of periphery burning and scattered fires, such as in central Haryana and northern Punjab (Figures 6, S4). Over the 5-year period from 2012-2016, VIIRS detected active fires in 73% of the 0.03° x 0.03° grid cells in Punjab and Haryana, while MODIS only detected active fires in 61% of the area (Figure S4c). In addition, VIIRS detected that 51% of grid cells burned consecutively during post-monsoon from 2012-2016, while MODIS detected only 31% of grid cells by this criterion.

Next, we compare district-level burned area from previous estimates (PRSC 2015; Yadav et al. 2014a; 2014b) to $BA_{ModL2T}$. Total Punjab $BA_{ModL2T}$ is 5% lower and 18% higher than that of PRSC (2015) in 2014 and 2015, respectively. In contrast, Punjab $BA_{MCD64A1}$ is lower than PRSC (2015) burned area estimates in both 2014 and 2015 by 20% and 3%, respectively (Figure S5). However, for northern Haryana districts, ModL2T and MCD64A1 both tend to overestimate burned area relative to Yadav et al. (2014a; 2014b). District-level $BA_{ModL2T}$ ($r = 0.88$, $p < 0.01$) and $BA_{MCD64A1}$ ($r = 0.87$, $p < 0.01$) are strongly correlated with PRSC (2015 and Yadav et al. (2014a; 2014b) burned area estimates. In terms of mean absolute error, ModL2T (257 $km^2$) outperforms MCD64A1 (279 $km^2$). However, MCD64A1 (slope = 1.03 ± 0.08) shows less overall bias than ModL2T (slope = 0.93 ± 0.07), which tends to overestimate burned area in Haryana districts relative to Yadav et al. (2014a; 2014b).

Finally, we assess 14-year trends and detrended interannual variations in mean post-monsoon MODIS AOD and $BA_{ModL2T}$. We find increased aerosol loading in ground-based column AOD measurements, during October-November, from the Aerosol Robotic Network (AERONET) site at Lahore (in the neighboring Pakistan province of Punjab) (Figure S6). Previous work of using HYSPLIT trajectories with MODIS FRP suggests that AOD weakly and positively co-varies with fire intensity during post-monsoon (Liu et al. 2018). Because the post-monsoon burning season spans the majority of October and November (Figure 5a) and aerosol loading from crop residue burning is temporally variable relative to other pollution sources, we assume that agricultural burning contributes to the majority of interannual variance in post-monsoon AOD over Punjab and Haryana. Due to potential long-range atmospheric transport of aerosols from the fire source region, we consider trends and interannual variability at coarse spatial scale. In the 14-year time span, satellite AOD increased by $0.017 \pm 0.003$ $yr^{-1}$ ($p < 0.01$) and $BA_{ModL2T}$ by $713 \pm 115$ $km^2$ $yr^{-1}$ ($p < 0.01$) (Figure S7a-b). While increased Landsat scene availability (Figure S1) may account for the some of the upward trend in $BA_{ModL2T}$, the upward trend in $BA_{MCD64A1}$, which has no dependency on Landsat, is higher at $966 \pm 84$ $km^2$ $yr^{-1}$ ($p < 0.01$) (Figure S7a). Additionally, regional $BA_{ModL2T}$ is weakly positively correlated with mean regional AOD for both the 3 km ($r = 0.39$, $p = 0.17$) and 10 km ($r = 0.36$, $p = 0.21$) datasets, but not statistically significant at the 99% confidence level (Figure S7c). Comparatively, $BA_{MCD64A1}$ is anti-correlated with mean regional AOD (3 km AOD: $r = -0.43$, $p = 0.13$; 10 km AOD: $r = -0.54$, $p < 0.05$) (Figure S7d).

### 3.3. Trends in landholding size and combine harvesters

The median landholding size in Haryana (1-2 ha) is smaller than that of Punjab (2-3 ha); only ~0.5% of landholdings in Haryana and ~1% in Punjab are over 20 ha (Figure 9). After some consolidation of small landholdings from 1995-96 to 2000-01, landholdings were increasingly fragmented from 2000-01 to 2010-11. Landholdings smaller than 7.5 ha increased from 88.2% to 89.5% of total landholdings in Haryana and 75.4% to 77.1% in Punjab from 2000-01 to 2010-11. Simultaneously, the number of combine harvesters tabulated by the Indian Input Survey increased 20-fold from 14 664 in 1996-97 to 297 132 in 2011-12 in Haryana and almost 3-fold from 93 191 in 1996-97 to 256 162 in 2011-12 in Punjab. In the 2016 household survey, 68% of surveyed farmers that used a combine harvester to harvest rice subsequently burned the crop residue in preparation for sowing wheat in Punjab and Haryana. Of those who burned crop residue, 93% used fully or partially mechanical methods of harvesting.

### 3.4. Two burning practices: size and shape of burn scars

Based on fine-resolution DigitalGlobe and CNES/Airbus historical imagery in November 2016, we observe two dominant crop residue burning practices in the study region that Kumar et al. (2015) observed in a field visit in Punjab: burning of (1) whole fields and (2) piled-up loose residue at the center of fields (Figure 10). Although farmers in Punjab and Haryana seem to employ a mixture of the two burning practices, available DigitalGlobe and CNES/Airbus images of the study region suggest that farmers in Punjab tend to fully burn fields and Haryana farmers both fully and partially burn fields post-harvest; Kumar et al. (2015) also concluded that whole-field burning is more popular in practice than partial burning in Punjab. Such distribution of the two burning practices suggest that whole field burning dominates the regional burned area contribution. Whole field burning induces dark scarring of entire fields such that adjoining fields burned in this way within days of each other are starkly contrasted against the surrounding unburned landscape (Figure 10a-b). In contrast, partial burning leaves circular or ring-shaped scarring in the center of fields; only ~1/9 of the field area is in fact scarred (Figure 10c-d).

# 4. Discussion

### 4.1. ModL2T-derived burned area: validation, assessments, and uncertainties

In this study, we use MODIS and Landsat imagery to estimate post-monsoon agricultural burned area in northwestern India for 14 years from 2003-2016. Use of Landsat imagery has been primarily limited by: (1) its low temporal resolution (16 days) and (2) storage and computing power. To minimize these limitations, we implement a hybrid MODIS-Landsat approach in Google Earth Engine, a cloud-computing platform with petabyte-scale storage, to rapidly process large collections of MODIS and Landsat imagery and expand the spatio-temporal range of study.

Here we aim to improve $BA_{MCD64A1}$ by extrapolating from the MCD64A1 training data, which we assume to be valid, and adding Landsat SR as an input. Because MCD64A1 performs relatively poorly in agricultural regions, we caution that use of MCD64A1 as a training dataset should be amended with availability of ground data or fine-resolution multispectral imagery (Giglio 2015; Hall et al. 2016; Zhu et al. 2017; Lasko et al. 2017; Fornacca et al. 2017). However, unlike the heterogenous, and even mountainous, topography associated with croplands in Russia (Hall et al. 2016; Zhu et al. 2017), Yunnan, China (Fornacca et al. 2017), and Hanoi province, Vietnam (Lasko et al. 2017) that increases the difficulty of burned area classification, the topography on which Punjab and Haryana croplands are situated is relatively homogenous and flat. Despite the small size of landholdings in Punjab and Haryana, fine-resolution Digital Globe and CNES/Airbus imagery reveals that clusters of fields are often burn within the same post-monsoon season, thus aggregating the size of otherwise relatively small burn scars. Further, ModL2T improves on MCD64A1 from the spatial resolution rather than the algorithm perspective. The higher average contribution of Landsat-only $BA_{ModL2T}$ (33%) over MODIS-only $BA_{ModL2T}$ (6%) to overall $BA_{ModL2T}$ confirms that additional burned area from ModL2T relative to MCD64A1 is primarily driven by integration of Landsat imagery rather differences in the ModL2T and MCD64A1 algorithms. Additionally, we find that incorporating Landsat imagery can improve the spatial allocation of small fires in northwestern India, which is important for modeling studies in which small fire emissions in close proximity can significantly impact the air quality estimates at a given location downwind. As such, $BA_{ModL2T}$ can be used as an experimental small fires boost for Punjab and Haryana.

In comparison to MCD64A1, the ModL2T algorithm estimates on average 66 ± 31% higher burned area in Haryana and Punjab during post-monsoon, from 2003-2016. We validate the $BA_{ModL2T}$ with survey data from 2016. The higher correlation ($r = 0.62$, $p < 0.01$) between village-level fractions of households that burn crop residue, normalized by landholding area, and $BA_{ModL2T}$, compared to $BA_{MCD64A1}$ ($r = 0.54$, $p < 0.01$), of total village cropland area suggests that the ModL2T algorithm can estimate burned area with increased accuracy. According to this validation, both ModL2T and MCD64A1 tend to underestimate burned area in northern Punjab villages and overestimate that in northeastern Haryana villages. The homogenous definition of the time range for pre-fire and post-fire collections for the ModL2T algorithm may have restricted burned scar detection. For example, the northern Punjab districts of Kapurthala and Jalandhar tend to burn earlier than other districts. Thus, more spatially dynamic temporal specifications of the pre-fire and post-fire image collections and detailed knowledge of the cropping patterns may decrease omission errors.

In additional assessments, we find that $BA_{ModL2T}$ improves on $BA_{MCD64A1}$ in terms of omission error, comparison with previous estimates of burned area, and relationship with satellite AOD. First, we find that $BA_{ModL2T}$ captures 95-100% of VIIRS active fires within its extent, while $BA_{MCD64A1}$ is only co-located with 69-76% of VIIRS active fires. Second, $BA_{ModL2T}$ improves on $BA_{MCD64A1}$ in terms of mean absolute error relative to previous district-level burned area estimates (PRSC 2015; Yadav et al. 2014a; 2014b). The strong overall agreement ($r$ = 0.87-0.88, $p < 0.01$) with PRSC (2015) and Yadav et al. (2014a; 2014b) burned area suggests that the ModL2T and MCD64A1 can achieve burned area estimates similar to methods using high-resolution satellite imagery, supervised classification, and ground truth validation at the district-level. While overall bias is higher in $BA_{ModL2T}$ than $BA_{MCD64A1}$ relative to previous estimates, the mean absolute error of $BA_{ModL2T}$ is lower. Finally, we find commensurate increasing trends in burned area and satellite AOD from 2003-2016, suggesting increasing fire activity and hazier conditions over the region during post-monsoon. Crop residue burning in Punjab and Haryana is a major source of regional pollution and driver of satellite AOD variability during post-monsoon months, influencing even aerosol properties and air quality of urban areas downwind (Kaskaoutis et al., 2014; Liu et al. 2018). Similar to Liu et al. (2018), we find that $BA_{ModL2T}$ exhibits a weak positive correlation with satellite AOD, after detrending, in contrast to the anti-correlation observed with $BA_{MCD64A1}$.

Of course, these validation and assessments are also subject to various limitations and uncertainties. For example, the 2016 household survey is spatially constrained to northeastern Haryana and northern Punjab and may be not representative of entire villages, as some villages have a small sample size. Without in-field GPS data and more detailed information on burn practices, we did not take into account partial burning and assumed a field is entirely burned if a farmer affirms crop residue burning. Similar to MODIS, VIIRS active fires are limited by satellite overpass times, the short burn duration of agricultural fires, and cloud or thick haze obscuration of fires. For pile burning, in which most of the field is left unburned, VIIRS will more readily detect these small fires based on thermal anomalies, which results in a lower detection threshold than the SR-based burned area classification. For such cases, burned area commission errors will be incorrectly treated as omission errors, which may explain the differences in VIIRS omissions errors despite relatively close agreement in the survey validation and assessment with previous studies. Further, by only using satellite imagery with high spatial resolution but low temporal resolution, PRSC (2015) and Yadav et al. (2014a; 2014b) burned area estimations are more susceptible to cloud and haze contamination and limited usable scenes. Finally, satellite AOD can be influenced by other local and regional post-monsoon pollution sources, such as urban and industrial emissions and Diwali festival fireworks (Cusworth et al. 2018). While the % valid pixels used for estimating mean regional AOD is relatively consistent across years (38 ± 3%), Cusworth et al. (2018) found that the MODIS cloud algorithm confuses thick haze with clouds, implying underestimation of AOD for days with severe haze, as in November 2016.

### 4.2. Limitations of burned area algorithms in northwestern India

$BA_{MCD64A1}$, which the GFEDv4s fire emissions inventory relies on, is derived from MODIS, a moderate-resolution satellite (500 m). In India, however, the average landholding tends to be comparatively small and fragmented (Misri 1999). In Punjab and Haryana, only 0.5-1% of landholdings are > 20 ha, comprising just 7-8.6% of total area. Because prescribed agricultural burning is constrained by landholding size, the estimation of small fire burned area is important in Punjab and Haryana. The Randerson et al. (2012) and van der Werf et al. (2017) approach for estimating the small fires contribution in GFEDv4s relies on two ratios: (1) $FC_{out}/FC_{in}$, or the ratio of active fires outside to those inside the $BA_{MCD64A1}$ extent for each 0.25° x 0.25° grid cell and (2) $(dNBR_{out} - dNBR_{control})/(dNBR_{in} - dNBR_{control})$, or the ratio that represents the dNBR outside and inside $BA_{MCD64A1}$ relative to an unburned control area. This methodology assumes confidence in $BA_{MCD64A1}$ to be from more spatially expansive fires and a linear correlation of burn severity with burned area (Randerson et al. 2012). However, unlike wildfires, whose burn severity and burned area extent can vary greatly, cropland fires are usually controlled in burn rate, time, and area, thus limiting the upper bound of burn severity and burned area extent per fire. For cropland fires, dNBR has been used more as a threshold for burned area classification rather than a proxy for burn severity (e.g. McCarty et al. 2008; 2009; Oliva and Schroeder 2015; Zhu et al. 2017). However, the downward trajectory of NBR is influenced by both harvest and burning (Hall et al. 2016). Clearly attributing decreases in NBR to burning remains challenging due to noise and gaps in NBR timeseries. In northwestern India, the time pressures of the double-crop system force a quick harvest-to-sowing turnaround time during post-monsoon, so burning may closely follow harvest (Kumar et al. 2015). Thus, the 16-day composite MOD13A1 SR product may be too temporally coarse for cropland dNBR in that it collects the best quality pixels and could miss the lowest NBR pixels immediately post-fire.

Moreover, based on the two dominant types of burning practices (whole and partial field burning) as seen in DigitalGlobe images of Punjab and Haryana during the post-monsoon burning season, pile burning (particularly in Haryana) may be more difficult to detect due to sub-landholding size fires. Of course, this difficulty is compounded by small median landholding sizes in Haryana (1-2 ha) and Punjab (2-3 ha). Particularly in Haryana, the potential prevalence of partial burning, in conjunction with small median landholding size (1-2 ha), makes it more difficult for moderate-resolution satellites to detect agricultural fires and accurately estimate burned area. Pile burning only scars the center of fields (~1/9 of field area), while whole field burning blackens the entire field. Thus, if a GFED grid cell contains a small sample of large or small fires, the dNBR ratio used in the small fire boost algorithm may be inaccurate. Similarly, if no or little $BA_{MCD64A1}$ is present within a grid cell, the potential of the small fires boost is limited. These challenges, some region-specific, are reflected in the performance of the GFEDv4s small fires boost (Randerson et al. 2012; van der Werf et al. 2017): added small fires emissions from 2003-2016 average ~20% of total post-monsoon Punjab and Haryana emissions, compared to ~47% of annual global agricultural emissions.

Finally, GFEDv4s and MCD64A1, both of which use active fire detections, are by extension susceptible to spatio-temporal limitations in MODIS satellite overpass times and detection limit. In India, agricultural fires typically last no more than half an hour (Thumaty et al. 2015). VIIRS, at a higher resolution (375 m), detected ~20% more 0.03º x 0.03º grid cells with active fires than MODIS/Terra and Aqua from 2012-2016. Even so, VIIRS would not be able detect small and cool fires and fires below optically hazy areas and outside of its overpass time. For example, if the peak fire energy is close to the late afternoon time (4:30 pm local time) estimated by Giglio (2007), the earlier daytime overpass times of MODIS/Terra and Aqua (10:30 am and 1:30 pm, respectively) and VIIRS (1:30 pm) imply missed fire detections. Oliva and Schroeder (2015) show that VIIRS-derived burned area compares poorly to a Landsat 8 reference dataset; in north India, the VIIRS fire detection rate was only 7.75% for fires < 10 ha and 28.82% for those > 10 ha.

Due to the short time window to detect burn scars and region-specific limitations, namely landholding size and variations in burning practices, sub-weekly, sub-Landsat resolution imagery is required to fine-tune burned area estimates at the landholding level. The low temporal availability of Landsat increases its susceptibility to low pixel availability from haze and clouds. Several scenes cover the study region, and the mismatch in date acquired may cause incongruity if one scene is hazy and cloudy. Further, although we use MOD09A1 (8-day composite) as the surface reflectance product instead of MOD13A1 (16-day composite) used in Randerson et al. (2012) and van der Werf et al. (2017), MOD09A1 may still be too coarse in temporal resolution. Thus, the limited overpass frequency of available satellite imagery from MODIS and Landsat suggests that the burned area estimates in this study are still likely conservative.

### 4.3. Implications of groundwater policy, increasing mechanization and land fragmentation

In 2009, the Punjab and Haryana governments implemented the "Preservation of Sub-soil Water Act, 2009" (Ordinance in 2008) to counteract groundwater depletion by delaying rice transplanting to after June 10 and 15, respectively. In effect, this policy forces the rice harvest season to extend to mid-November (Bhullar and Bhullar 2013; Singh 2009; PRSC 2015). Based on the 2016 household survey, 76% of farmers in Punjab and Haryana ideally prefer to sow wheat before November 15, but only 44% were able to sow wheat before mid-November. This ideal-actual sow date difference is starker for farmers who burned crop residue: 78% prefer to sow before mid-November, but only 35% sowed before this date. We find an average step increase of ~28% in $BA_{ModL2T}$ from the 2003-07 to 2008-16 time period. A two-sample t-test shows that the difference in $BA_{ModL2T}$ between the two time periods is statistically significant ($p < 0.01$) with a mean difference of 5762 km$^2$ (95% CI: [3086, 8438] km$^2$). However, further work is needed to robustly quantify the effect of potential delays in rice harvests and agricultural fires on a finer temporal scale, or daily to weekly basis.

In northwestern India, agricultural mechanization, combined with the time-intensive double-crop system, drives crop residue burning. Combine harvesters, normalized by total landholdings, increased by 58% from 2001-02 to 2011-12. However, at the same time, % landholdings < 7.5 ha increased by ~1.5% from 2000-01 to 2010-11 in Punjab and Haryana. Increasing land fragmentation may slow the rate of agricultural mechanization as marginal and small landholdings become too fragmented to be mechanized or mechanized in the same way as medium and large landholdings (Deininger et al. 2017; Mehta et al. 2014). Specifically, the widening technology gap between marginal to small (manual and animal-drawn) and medium to large (tractor-drawn and self-propelled) landholdings may be reduced through consolidation (Mehta et al. 2014). However, if consolidation efforts strengthen as a result of the demand for higher crop productivity and agricultural mechanization, crop residue burning rates may accelerate unless alternative, more sustainable methods become viable and cost-time effective.

### 4.4. Future directions for burned area mapping and fire emissions inventories

The recent proliferation of finer resolution satellites, such as VIIRS (375 m, daily, post-2012), Sentinel-2 (10-20 m, every 5 days, post-2015) and Planet (<5 m, daily, post-2016), offers added potential for active fire and burn scar detection (Drusch et al. 2012; Strauss 2017). Integration of these products with the hybrid MODIS-Landsat framework can improve accuracy in burned area estimation and fire emissions inventories for more recent years of study (e.g. Wang et al. 2017). For example, the emissions factor for partial burning may be higher than whole field burning, but its burn scar is sub-landholding size and its emissions footprint is therefore difficult to estimate even at Landsat resolution. Fine-resolution sensors can be used to distinguish the spatial patterns of the burning practices to better inform fire emissions inventories retroactively and proactively. Additionally, the coupling of cloud computing and geospatial datasets in GEE makes near-real time analysis possible for policy and management decisions (Gorelick et al. 2017). Rapid availability of updated collections of satellite-derived products on GEE can decrease the turnover time for new versions of fire emissions inventories, such as GFEDv4s, which currently uses MCD64A1 C5.1 (van der Werf et al. 2017). Finally, our reliance on MCD64A1 as a training dataset in the absence of a spatio-temporally expansive ground truth dataset signals a need for collection of detailed multi-year survey data on crop residue burning in northwestern India. Due to high uncertainties associated with small cropland fires, we recommend that global burned area and fire emissions datasets integrate ground truth data in northwestern India to train and validate algorithms.

## 5. Conclusion

The two-fold problem of satellite spatial and temporal limitations poses a difficult challenge for estimating burned area from agricultural fires. In particular, the small landholdings in the region and the short duration of agricultural fires require both high spatial and temporal satellite resolution. MODIS burned area product MCD64A1 is limited by moderate spatial resolution (500 m), and the GFEDv4s small fires boost to MCD64A1 further limits the spatial resolution (0.25°). In this study, we develop a hybrid approach (ModL2T) that leverages the temporal resolution of MODIS (daily, 500 m) and spatial resolution of Landsat (every 16 days, 30 m) in a two-step NBR-based classification. Additionally, we use the Google Earth Engine platform to rapidly run the ModL2T algorithm using all available MODIS and Landsat images within the defined pre-fire and post-fire time periods to classify post-monsoon (October to November) burned area. The ModL2T algorithm estimates 66 ± 31% higher post-monsoon burned area than MCD64A1 in Punjab and Haryana from 2003-2016. In future work, the high-resolution $BA_{ModL2T}$ (30 m) dataset, which moderately well agrees ($r = 0.62$) with independent household survey results, can be used to boost emissions from small post-monsoon agricultural fires in Punjab and Haryana and re-evaluate – and likely previously underestimated – regional public health effects. Lastly, the methods described in this study may be useful in other regions with high concentrations of small fires and in improving global fire emissions inventories currently based on moderate-resolution satellite products.

## Acknowledgements

We acknowledge the Columbia University Department of Earth and Environmental Sciences Young Investigator Award and Earth Institute Research Assistantship program for support for this work, as well as the Columbia University President's Global Innovation Fund. This work was also supported by a National Science Foundation Graduate Research Fellowship awarded to T.L. (Award Number DGE1144152 and DGE1745303). The household survey in 2016 was funded by a NSF SEES Postdoctoral Fellowship (Award Number 1415436) to M.J. We also thank Dr. Brent Holben and site managers for establishing and maintaining AERONET Lahore, Pakistan site.

## References

Ahmed, T., B. Ahmad, and W. Ahmad (2015). Why do farmers burn rice residue? Examining farmers' choices in Punjab, Pakistan. *Land Use Policy*, 47, 448-458. doi:10.1016/j.landusepol.2015.05.004.

Avery, T. E. and G. L. Berlin (1992). *Fundamentals of remote sensing and airphoto interpretation.* Upper Saddle River: Prentice Hall.

Bai, R. (2014). Analysis of the Trends of Agricultural Mechanization Development in China (2000-2020). *ESCAP/CSAM Policy Brief*, Issue No.1. http://www.un-csam.org/publication/PB201401.pdf.

Bhullar, G. S. and N. K. Bhullar (2013). *Agricultural Sustainability: Progress and Prospects in Crop Research*. London: Academic Press/Elsevier.

Boschetti, L., D. P. Roy, C. O. Justice, and M. L. Humber (2015). MODIS–Landsat fusion for large area 30 m burned area mapping. *Remote Sensing of Environment*, 161, 27-42. doi:10.1016/j.rse.2015.01.022.

Chen, J., Y. Ban, and S. Li (2014). Open access to Earth land-cover map. *Nature*, 514, 434. doi:10.1038/514434c.

Chen, J., Cao, X., Peng, S., and Ren, H. (2017). Analysis and Applications of GlobeLand30: A Review. *International Journal of Geo-Information*. 6, 230. doi:10.3390/ijgi6080230.

Cocke, A. E., P. Z. Fulé, and J. E. Crouse (2005). Comparison of burn severity assessments using Differenced Normalized Burn Ratio and ground data. *International Journal of Wildland Fire* 14(2), 189-198. doi:10.1071/WF04010.

Cohen, J. (1960). A coefficient of agreement for nominal scales. *Education and Psychological Measurement*, 20, 37-46. doi:10.1177/001316446002000104.

Cusworth, D. H., L. J. Mickley, M. P. Sulprizio, T. Liu, M. E. Marlier, R. S. DeFries, S. K. Guttikunda, and P. Gupta (2018). Quantifying the influence of agricultural fires in northwest India on urban air pollution in Delhi, India. *Environmental Research Letters*, 13, 044018. doi:10.1088/1748-9326/aab303.

Deininger, K., D. Monchuk, H. K. Nagarajan, and S. K. Singh (2017). Does Land Fragmentation Increase the Cost of Cultivation? Evidence from India. *The Journal of Development*

*Studies*, 53, 82-98. doi: 10.1080/00220388.2016.1166210.

Drusch, M., U. Del Bello, S. Carlier, O. Colin, V. Fernandez, F. Gascon, B. Hoersch, C. Isola, P. Laberinti, P. Martimort, A. Meygret, F. Spoto, O. Sy, F. Marchese, and P. Bargellini (2012). Sentinel-2: ESA's optical high-resolution mission for GMES operational services. *Remote Sensing of Environment* 120, 25-36. doi: 10.1016/j.rse.2011.11.026

Eva, H. and E. F. Lambin (1998). Burnt area mapping in Central Africa using ATSR data. *International Journal of Remote Sensing*, 19, 3473-3497. doi:10.1080/014311698213768.

Fornacca, D., G. Ren, and W. Xiao (2017). Performance of Three MODIS Fire Products (MCD45A1, MCD64A1, MCD14ML), and ESA Fire_CCI in a Mountainous Area of Northwest Yunnan, China, Characterized by Frequent Small Fires. *Remote Sensing*, 9, 1131. doi:10.3390/rs9111131.

Giglio, L. (2007). Characterization of the tropical diurnal fire cycle using VIRS and MODIS observations. *Remote Sensing of Environment*, 108, 407-421. doi:10.1016/j.rse.2006.11.018.

Giglio, L., T. Loboda, D. P. Roy, B. Quayle, and C. O. Justice (2009). An active-fire based burned area mapping algorithm for the MODIS sensor. *Remote Sensing of Environment* 113, 408-420. doi:10.1016/j.rse.2008.10.006.

Giglio, L., J. T. Randerson, and G. R. van der Werf. 2013. "Analysis of daily, monthly, and annual burned area of the fourth-generation global fire emissions database (GFED4)." *Journal of Geophysical Research*, 118, 317-328. doi:10.1002/jgrg.20042.

Giglio, L. (2015). MODIS Collection 6 Active Fire Product User's Guide Revision A. https://cdn.earthdata.nasa.gov/conduit/upload/3865/MODIS_C6_Fire_User_Guide_A.pdf

Giglio, L., L. Boschetti, D. Roy, A. A. Hoffmann, and M. Humber (2016). Collection 6 MODIS Burned Area Product User's Guide Version 1.0. http://modis-fire.umd.edu/files/MODIS_C6_BA_User_Guide_1.0.pdf

Gorelick, N., M. Hancher, M. Dixon, S. Ilyushchenko, D. Thau, and R. Moore (2017). Google Earth Engine: Planetary-scale geospatial analysis for everyone. *Remote Sensing of Environment*, 202, 18-27. doi:10.1016/j.rse.2017.06.031.

Government of Punjab (2007). *State of environment*. Chandigarh: Punjab State Council of Science and Technology.

Gupta, R. (2012). *Causes of Emissions from Agricultural Residue Burning in North-West India: Evaluation of a Technology Policy Response.* SANDEE Working Paper No. 66–12.

Hall, J. V., T. V. Loboda, L. Giglio, and G. W. McCarty (2016). A MODIS-based burned area assessment for Russian croplands: Mapping requirements and challenges. *Remote Sensing of Environment*, 184, 506-521.

Jain, N., A. Bhatia, and H. Pathak (2014). Emission of Air Pollutants from Crop Residue Burning in India. *Aerosol and Air Quality Research*, 14, 422-430. doi:10.4209/aaqr.2013.01.0031.

Kaskaoutis, D. G., S. Kumar, D. Sharma, R. P. Singh, S. K. Kharol, M. Sharma, A. K. Singh, S. Singh, A. Singh, and D. Singh (2014). Effects of crop residue burning on aerosol properties, plume characteristics, and long-range transport over northern India. *Journal of Geophysical Research*, 119, 5424-5444. doi: 10.1002/2013JD021357.

Key, C. H. and N. C. Benson (2006). Landscape assessment (LA): Sampling and analysis methods. In D. C. Lutes, R. E. Keane, J. F. Caratti, C. H. Key, N. C. Benson, S. Sutherland, and L .J. Gangi (Eds.). *FIREMON: Fire effects monitoring and inventory system*. General Technical Report RMRS-GTR-164-CD (pp. LA1−LA51). Rocky Mountain Research Station, Fort Collins, CO: United States Department of Agriculture, Forest Service. http://www.fs.fed.us/rm/pubs/rmrs_gtr164.pdf.

Kumar, P., S. Kumar, and L. Joshi (2015). *Socioeconomic and Environmental Implications of Agricultural Residue Burning: A Case Study of Punjab, India*.

Landis, J. R. and G. G. Kock (1977). “=The Measurement of Observer Agreement for Categorical Data. *Biometrics*, 33, 159-174. doi:10.2307/2529310.

Lasko, K., K. P. Vadrevu, V. T. Tran, E. Ellicott, T. T. N. Nguyen, H. Q. Bui, and C. Justice (2017). Satellites may underestimate rice residue and associated burning emissions in Vietnam. *Environmental Research Letters*, 12, 085006. doi:10.1088/1748-9326/aa751d.

Levy, R. C., S. Mattoo, L. A. Munchak, L. A. Remer, A. M. Sayer, F. Patadia, and N. C. Hsu. (2013). The Collection 6 MODIS aerosol products over land and ocean. *Atmospheric Measurement Techniques*, 6, 2989-3034. doi:10.5194/amt-6-2989-2013.

Lewis, S. A., A. T. Hudak, R. D. Ottmar, P. R. Robichaud, L. B. Lentile, S. M. Hood, J. B. Cronan, and P. Morgan (2011). Using hyperspectral imagery to estimate forest floor consumption from wildfire in boreal forests of Alaska, USA. *International Journal of Wildland Fire*, 20, 255-271. doi:10.1071/WF09081.

Liu, T., M. E. Marlier, R. S. DeFries, D. M. Westervelt, K. R. Xia, A. M. Fiore, L. J. Mickley, D. H. Cusworth, and G. Milly (2018). Seasonal impact of regional outdoor biomass burning on air pollution in three Indian cities: Delhi, Bengaluru, and Pune. *Atmospheric Environment*, 172, 83-92. doi:10.1016/j.atmosenv.2017.10.024.

Loboda, T., K. J. O’Neal, and I. Csiszar (2007). Regionally adaptable dNBR-based algorithm for burned area mapping from MODIS data. *Remote Sensing of Environment*, 109, 429-442. doi:10.1016/j.rse.2007.01.017.

Mahajan, G., V. Kumar, and B. S. Chauhan (2017). Rice Production in India. In: B. Chauhan, K. Jabran, G. Mahajan G. (eds). *Rice Production Worldwide*. Springer, Cham. doi:10.1007/978-3-319-47516-5_3.

McCarty, J. L., S. Korontzi, and S. Trigg (2008). A hybrid remote sensing approach to quantifying crop residue burning in the United States. *Applied Engineering in Agriculture*, 24, 515-527. doi:10.13031/2013.25137.

McCarty, J. L., S. Korontzi, C. O. Justice, and T. Loboda (2009). The spatial and temporal distribution of crop residue burning in the contiguous United States. *Science of The Total Environment*, 407, 5701-5712. doi:10.1016/j.scitotenv.2009.07.009.

Mehta, C. R., N. S. Chandel, T. Senthilkumar, and K. K. Singh (2014). Trends of Agricultural Mechanization in India. *ESCAP/CSAM Policy Brief*, Issue No. 2. http://www.un-csam.org/publication/PB201402.pdf.

Misri, B. K. (1999). *Country Pasture/Forage Resources Profiles, India.* http://www.fao.org/ag/AGP/AGPC/doc/Counprof/India.htm.

Mu, M., J. T. Randerson, G. R. van der Werf, L. Giglio, P. Kasibhatla, D. Morton, G. J. Collatz, R. S. DeFries, E. J. Hyer, E. M. Prins, D. W. T. Griffith, D. Wunch, G. C. Toon, V. Sherlock, and P. O. Wennberg. (2011). Daily and 3-hourly variability in global fire emissions and consequences for atmospheric model predictions of carbon monoxide. *Journal of Geophysical Research: Atmospheres*, 116, D24303. doi:10.1029/2011JD016245.

Munchak, L. A., R. C. Levy, S. Mattoo, L. A. Remer, B. N. Holben, J. S. Schafer, C. A. Hostetler, and R. A. Ferrare (2013). MODIS 3 km aerosol product: applications over land in an urban/suburban region. *Atmospheric Measurement Techniques*, 6, 1747-1759. doi:10.5194/amt-6-1747-2013.

Oliva, P. and W. Schroeder (2015). Assessment of VIIRS 375 m active fire detection product for direct burned area mapping. *Remote Sensing of Environment*, 160, 144-155. doi:10.1016/j.rse.2015.01.010.

Picotte, J. J. and K. M. Robertson (2010). Accuracy of remote sensing wildland fire–burned area in southeastern U.S. Coastal Plain habitats. In K. M. Robertson, K. E. M. Galley, and R. E. Masters (eds.). *Proceedings of the 24th Tall Timbers Fire Ecology Conference: The Future of Prescribed Fire: Public Awareness, Health, and Safety. Tall Timbers Research Station, Tallahassee, Florida, USA.*

Pleniou, M. and N. Koutsias (2013). Sensitivity of spectral reflectance values to different burn and vegetation ratios: A multi-scale approach applied in a fire affected area. *ISPRS Journal of Photogrammetry and Remote Sensing*, 79, 199-210. doi:10.1016/j.isprsjprs.2013.02.016.

Punia, M., V. P. Nautiyal, and Y. Kant (2008). Identifying biomass burned patches of agriculture residue using satellite remote sensing data. *Current Science* 94, 1185-1190.

Punjab Remote Sensing Center (PRSC), Ludhiana (2015). *Monitoring Residue Burning through Satellite Remote Sensing.* Punjab Pollution Control Board, Patiala.

Randerson, J. T., Y. Chen, G. R. van der Werf, B. M. Rodgers, and D. C. Morton (2012). Global burned area and biomass burning emissions from small fires. *Journal of Geophysical Research*, 117, G04012. doi:10.1029/2012JG002128.

Rogan, J. and S. R. Yool (2001). Mapping fire-induced vegetation depletion in the Peloncillo Mountains: Arizona and New Mexico. *International Journal of Remote Sensing*, 22, 3101-3121. doi:10.1080/01431160152558279.

Roy, D. P. (1999). Multi-temporal active-fire based burn scar detection algorithm.” *International Journal of Remote Sensing*, 20, 1031-1038. doi:10.1080/014311699213073.

Roy, D. P., Y. Jin, P. E. Lewis, and C. O. Justice (2005). Prototyping a global algorithm for systematic fire-affected area mapping using MODIS time series data. *Remote Sensing of Environment*, 97, 137-162. doi:10.1016/j.rse.2005.04.007.

Sayer, A. M., N. C. Hsu, C. Bettenhausen, and M-J. Jeong (2013). Validation and uncertainty estimates for MODIS Collection 6 “Deep Blue” aerosol data. *Journal of Geophysical*

*Research: Atmospheres*, 118, 7864-7872. doi:10.1002/jgrd.50600.

Schroeder, W. and L. Giglio (2018). NASA VIIRS Land Science Investigator Processing System (SIPS) Visible Infrared Imaging Radiometer Suite (VIIRS) 375 m & 750 m Active Fire Products: Product User’s Guide Version 1.4” https://viirsland.gsfc.nasa.gov/PDF/VIIRS_activefire_User_Guide.pdf

Sharma, A. R., S. K. Kharol, K. V. S. Badarinath, and D. Singh (2010). Impact of agriculture crop residue burning on atmospheric aerosol loading – a study over Punjab State, India. *Annales Geophysicae*, 28, 367-379.

Sidhu, B. S., and V. Beri (2005). Experience with managing rice residues in intensive rice-wheat cropping system in Punjab. In I. P. Abrol, R. K. Gupta, and R. K. Malik (Eds.), *Conservation agriculture: Status and prospects* 55-63. New Delhi: Center for Advancement of Sustainable Agriculture, National Agriculture Science Center.

Singh, G., Y. Kant, and V. K. Dadhwal (2009). Remote sensing of crop residue burning in Punjab (India): a study on burned area estimation using multi-sensor approach. *Geocarto International*, 24, 273-292. doi:10.1080/10106040802556181.

Singh, K. (2009). Act to Save Groundwater in Punjab: Its Impact on Water Table, Electricity Subsidy and Environment. *Agricultural Economics Research Review*, 22, 365-386.

Singh, M. K., R. Gautam, and P. Venkatachalam (2017). Bayesian Merging of MISR and MODIS Aerosol Optical Depth Products Using Error Distributions From AERONET. *IEEE Journal of Selected Topics in Applied Earth Observations and Remote Sensing* 10, 5186-5200. doi:10.1109/JSTARS.2017.2734331.

Singh, R. P., H. S. Dhaliwal, H. S. Sidhu, Y. S. Manpreet-Singh, and J. Blackwell (2008). Economic assessment of the Happy Seeder for rice-wheat systems in Punjab, India. Conference Paper, AARES 52nd Annual conference, Canberra. Australia: ACT.

Strauss, M. (2017). Planet Earth to get a daily selfie. *Science*, 355, 782-783. doi:10.1126/science.355.6327.782.

Thumaty, K. C., S. R. Rodda, J. Singhal, R. Gopalakrishnan, C. S. Jha, G. D. Parsi, and V. K. Dadhwal (2015). Spatio-temporal characterization of agriculture residue burning in Punjab and Haryana, India, using MODIS and Suomi NPP VIIRS data. *Current Science* 109, 1850-1855. doi:10.18520/v109/i10/1850-1855.

Vadrevu, K. P., E. Ellicott, and K. Badarinath (2011). MODIS derived fire characteristics and aerosol optical depth variations during the agricultural residue burning season, north India. *Environmental Pollution*, 159, 1560-1569. doi:10.1016/j.envpol.2011.03.001.

van der Werf, G. R., J. T. Randerson, L. Giglio, G. J. Collatz, M. Mu, P. S. Kasibhatia, D. C. Morton, R. S. DeFries, Y. Jin, and T. T. van Leeuwen (2010). Global fire emissions and the contribution of deforestation, savanna, forest, agricultural, and peat fires (1997-2009). *Atmospheric Chemistry and Physics*, 10, 11707-11735. doi:10.5194/acp-10-11707-2010.

van der Werf, G. R, J. T. Randerson, L. Giglio, T. T. van Leeuwen, Y. Chen, B. M. Rogers, M. Mu, M. J. E. van Marle, D. C. Morton, G. J. Collatz, R. J. Yokelson, P. S. Kasibhatla. (2017). Global fire estimates during 1997-2016. *Earth System Science Data*, 9, 687-720. doi:10.5194/essd-2016-62.

Veraverbeke, S., W. W. Verstraeten, S. Lhermitte, and R. Goossens (2010). Illumination effects on the differenced Normalized Burn Ratio's optimality for assessing fire severity. *International Journal of Applied Earth Observation and Geoinformation*, 12, 60-70. doi:10.1016/J.JAG.2009.10.004.

Vermote, E. F. and S. Kotchenova (2008). Atmospheric correction for the monitoring of land surfaces. *Journal of Geophysical Research*, 113, D23S90. doi:10.1029/2007JD009662

United Nations, Department of Economic and Social Affairs, Population Division (2015). *World Population Prospects: The 2015 Revision, Key Findings and Advance Tables Working Paper No. ESA/P/WP.241*.

Wang, Q., G. A. Blackburn, A. O. Onojeghuo, J. Dash, L. Zhou, Y. Zhang, and P. M. Atkinson (2017). Fusion of Landsat 8 OLI and Sentinel-2 MSI Data. *IEEE Transactions on Geoscience and Remote Sensing*, 55, 3885-3899. doi: 10.1109/TGRS.2017.2683444.

Wang, S., M. H. A. Baig, S. Liu, H. Wan, T. Wu, and Y. Yang (2018). Estimating the area burned by agricultural fires from Landsat 8 Data using the Vegetation Difference Index and Burn Scar Index. *International Journal of Wildland Fire*, 27, 217-227. doi: 10.1071/WF17069.

Xiang, H.-B. (2013). Algorithms for Moderate Resolution Imaging Spectroradiometer cloud-free image compositing. *Journal of Applied Remote Sensing*, 7, 073486. doi: 10.1117/1.JRS.7.073486.

Yadav, M., M. P. Sharma, R. Prawasi, R. Khichi, P. Kumar, V. P. Mandal, A. Salim, and R. S. Hooda (2014a). "Estimation of Wheat/Rice Residue Burning Areas in Major Districts of Haryana, India, Using Remote Sensing Data." *Journal of the Indian Society of Remote Sensing*, 42, 343-352. doi:10.1007/s12524-013-0330-z.

Yadav, M., R. Prawasi, S. Jangra, P. Rana, K. Kumari, S. Lal, K. Jakhar, S. Sharma, and R. S. Hooda (2014b). Monitoring seasonal progress of rice stubble burning in districts of Haryana, India, using multidate AwiFS data. *The International Archives of the Photogrammetry, Remote Sensing and Spatial Information Sciences*, 40, 1003-1009. doi:10.5194/isprsarchives-XL-8-1003-2014.

Zhu, C., H. Kobayashi, Y. Kanaya, and M. Saito (2017). Size-dependent validation of MODIS MCD64A1 burned area over six vegetation types in boreal Eurasia: Large underestimation in croplands. *Scientific Reports*, 7, 4181. doi:10.1038/s41598-017-03739-0.

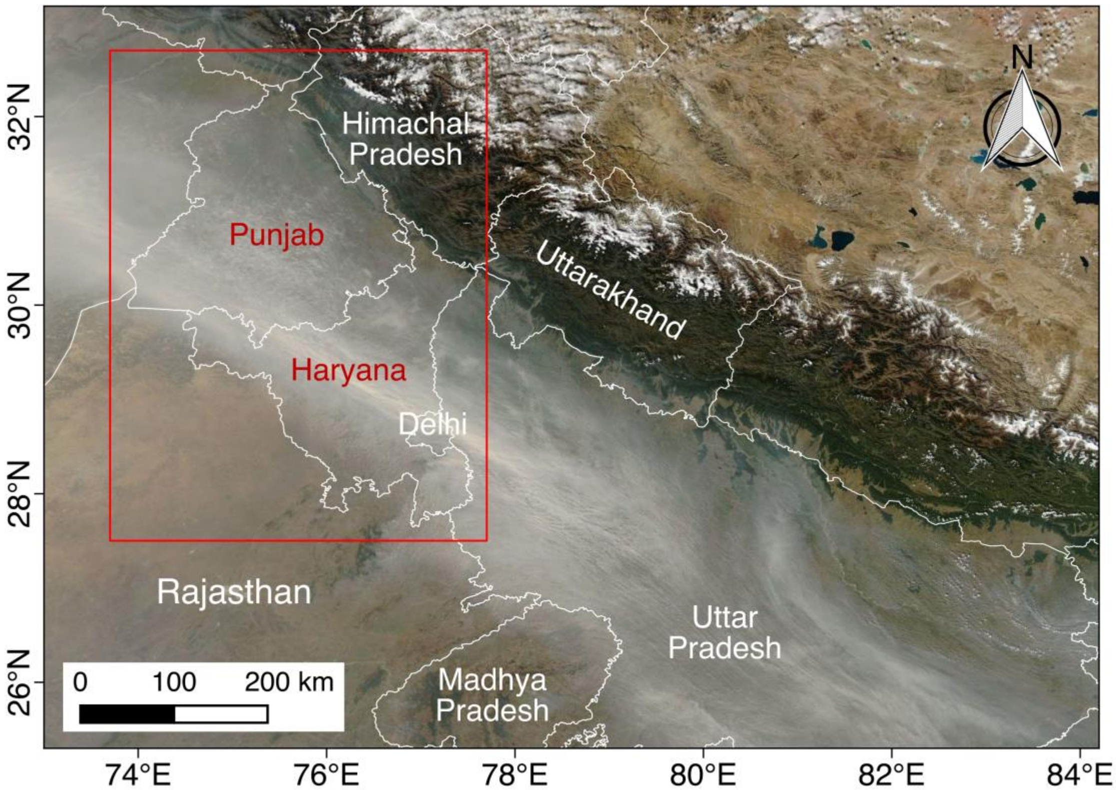


**Figure 1. Example of thick haze over northern India during the post-monsoon burning season**: True color MODIS/Aqua on November 6, 2016 (NASA Worldview). The study area is bounded by a red box.

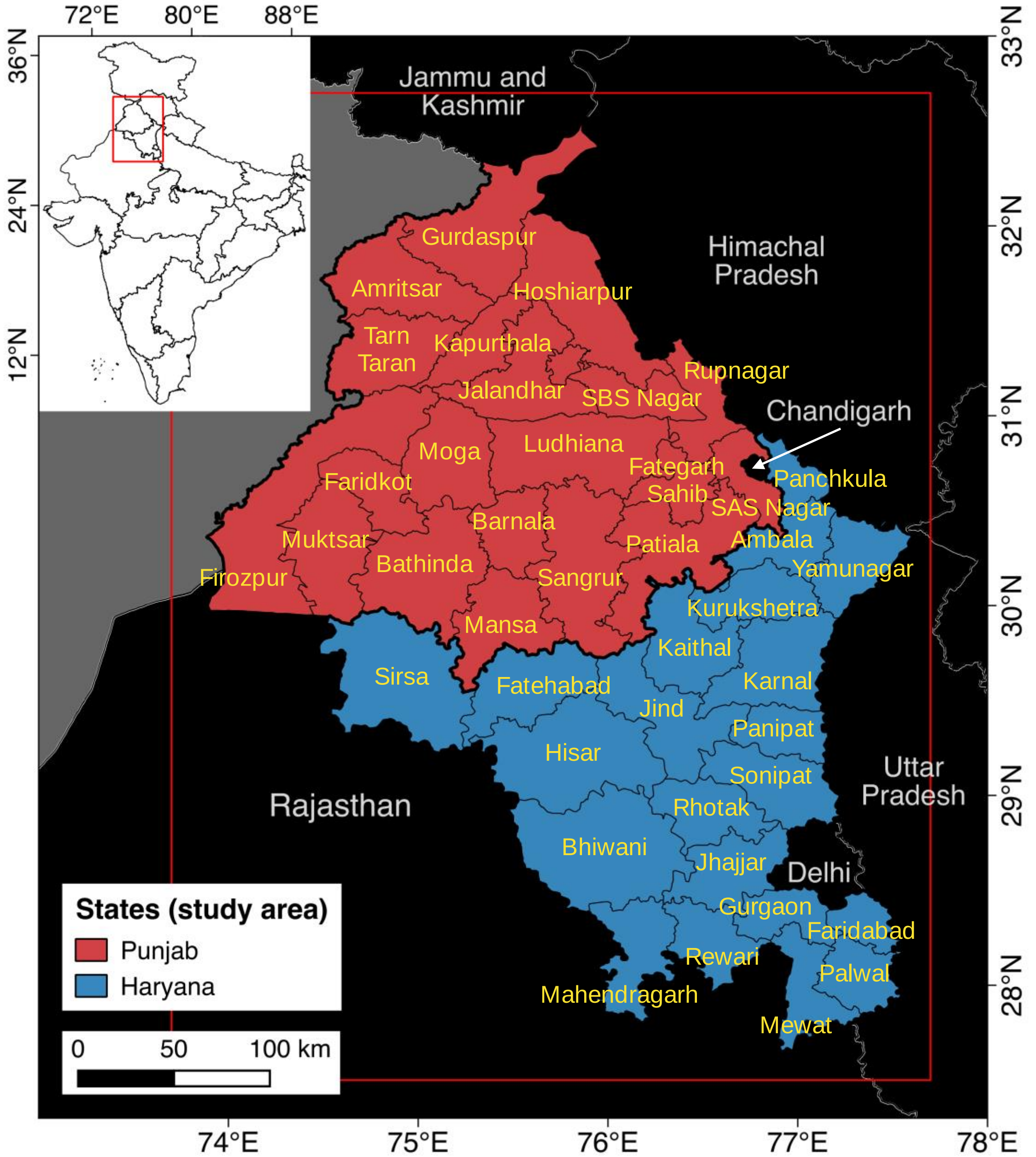


**Figure 2. District-level maps of the study area**: Punjab (red) and Haryana (blue), two agricultural states in northwestern India. District administrative borders are from the 2011 Indian census. *Inset*: The red box shows the location of the study area in a zoomed-out view of states in India, excluding the seven sister states.

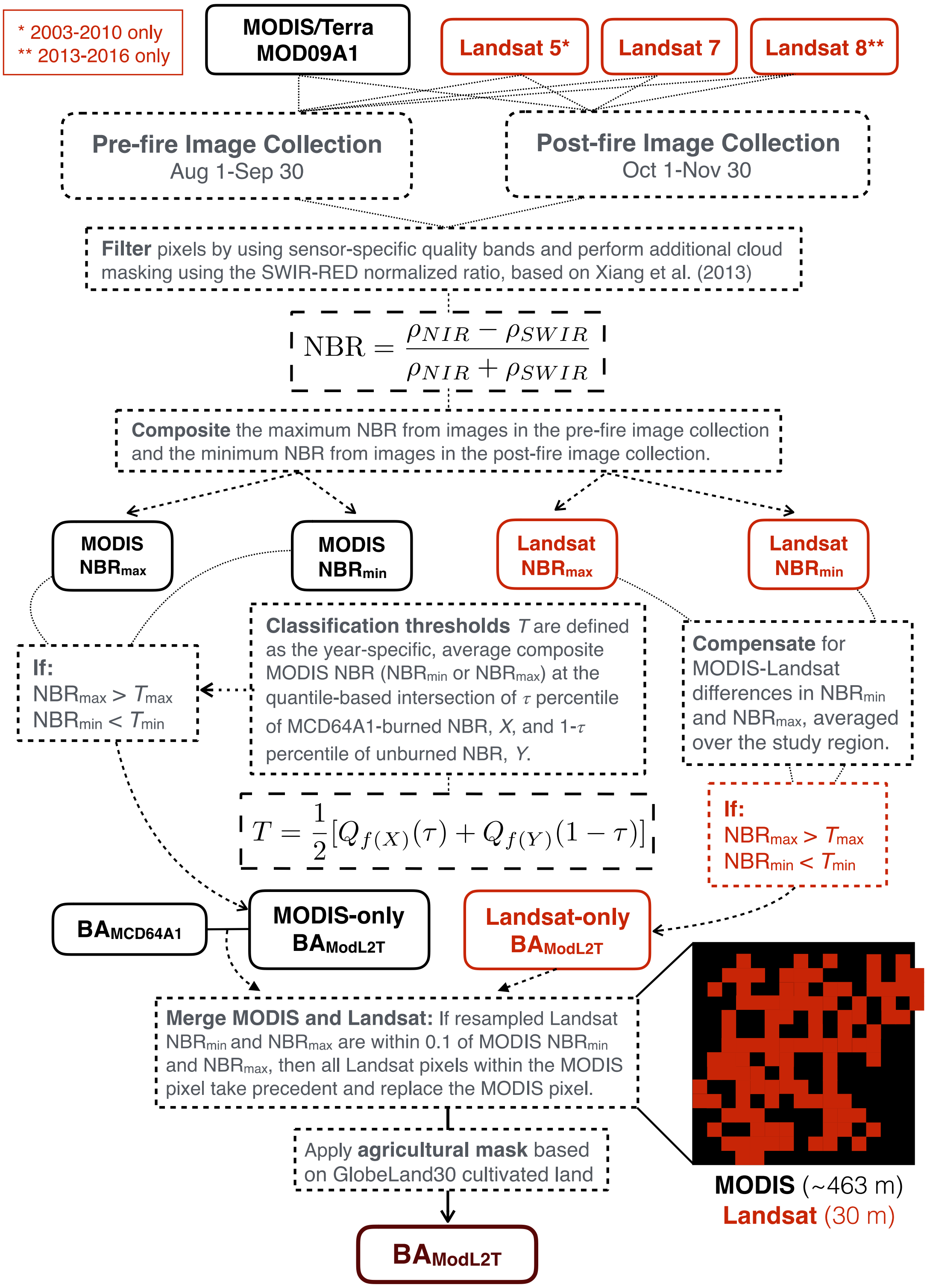


**Figure 3. Workflow of the ModL2T algorithm**: estimation of post-monsoon (October-November) agricultural burned area. The final ModL2T burned area is 30 m x 30 m in spatial resolution. The inset schematic shows Landsat burned pixels (red) overlain on a MODIS burned pixel (black); if the MODIS-Landsat merging criteria are met, then the ~238 Landsat pixels replace the MODIS pixel.

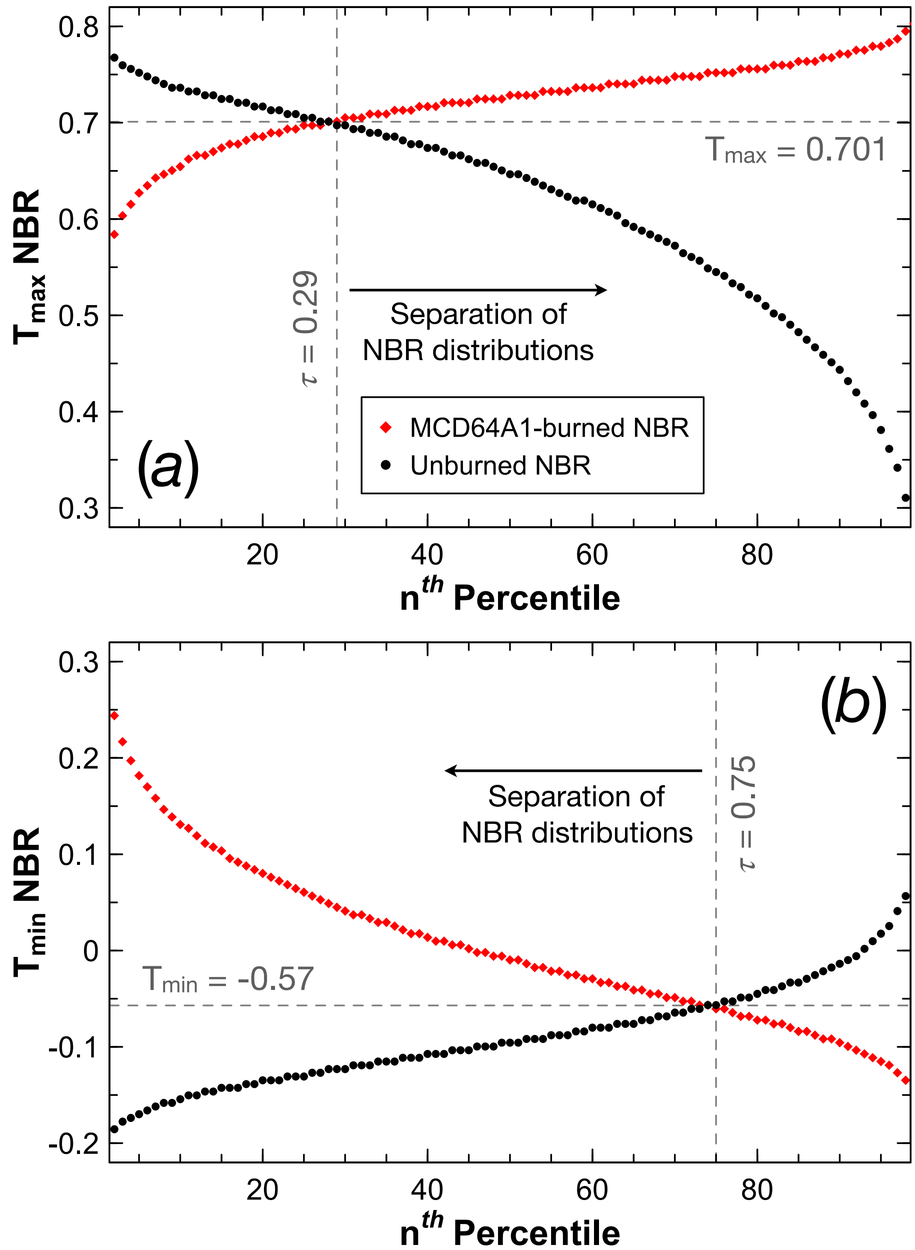


**Figure 4. Example of thresholds $T_{min}$ and $T_{max}$ derived for post-monsoon 2016**: thresholds $T_{min}$ and $T_{max}$ for the ModL2T algorithm (Figure 3) are derived from the $\tau$ percentile separation of MCD64A1-burned NBR and unburned NBR distributions in agricultural areas.

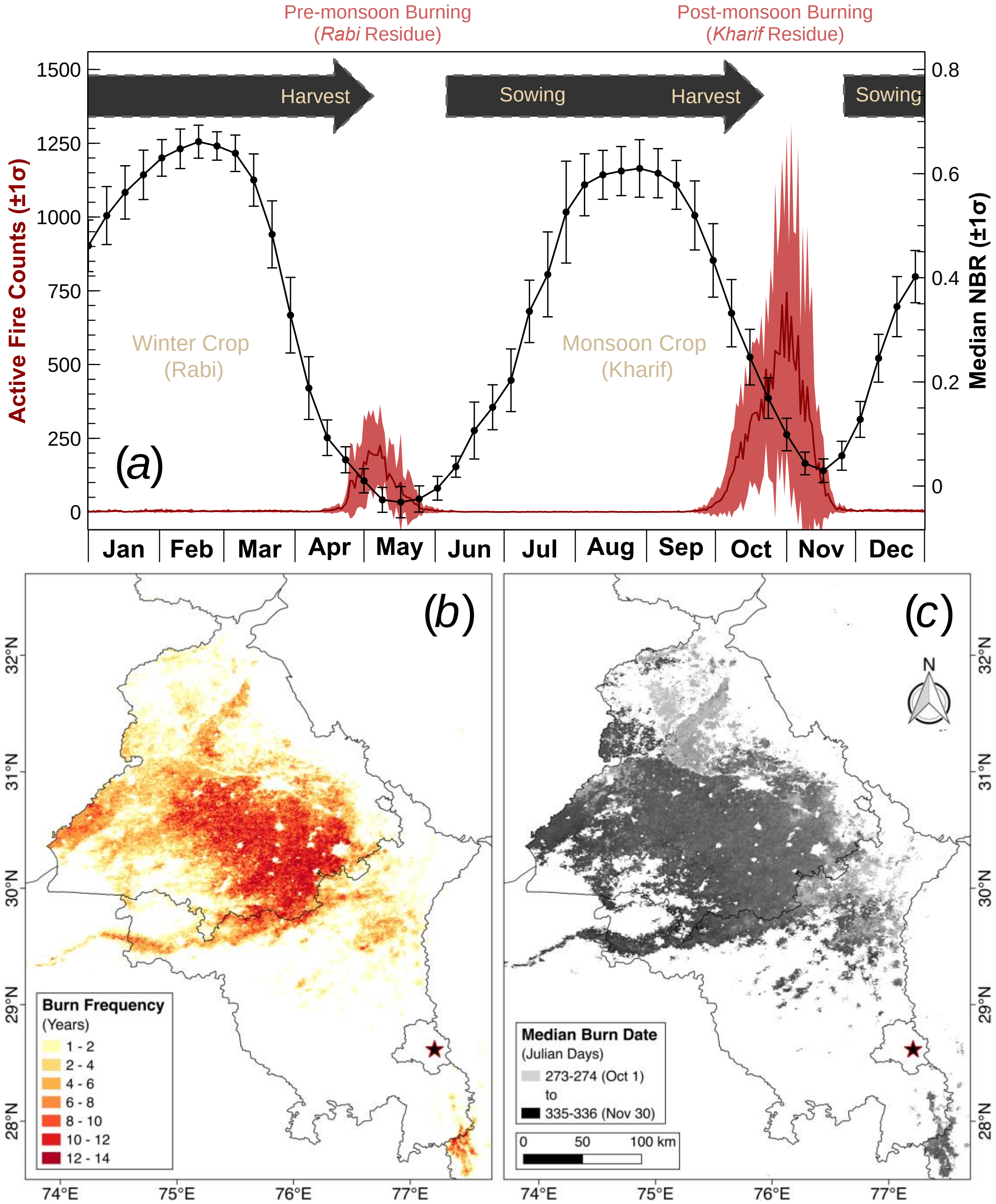


**Figure 5. Spatio-temporal overview of agricultural burning in northwestern India**: (*a*) The double crop-fire cycle, following Vadrevu et al. (2011), using daily MODIS fire counts and 8-day composite median NBR, with ±1σ envelopes, in Punjab and Haryana, 2003-2016. Post-monsoon (October-November) (*b*) burn frequency and (*c*) median burn date based on $BA_{MCD64A1}$. The color bar is discrete in (*b*) and continuous in (*c*). The star denotes the location of New Delhi.

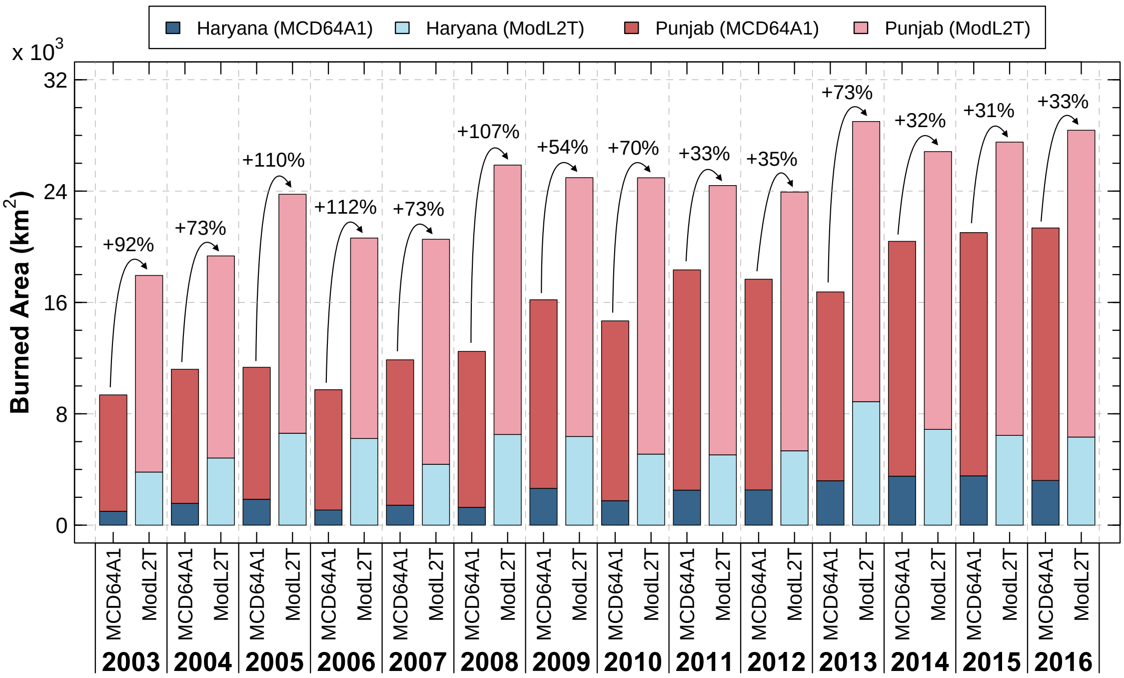


**Figure 6. Total agricultural burned area**: $BA_{MCD64A1}$ and $BA_{ModL2T}$ in Punjab (red shades) and Haryana (blue shades) during post-monsoon (October-November), 2003-2016. The ModL2T algorithm estimates 66 ± 31% higher post-monsoon burned area in Punjab and Haryana than MCD64A1. The curved arrows denote the relative increase in burned area mapped by ModL2T compared to MCD64A1.

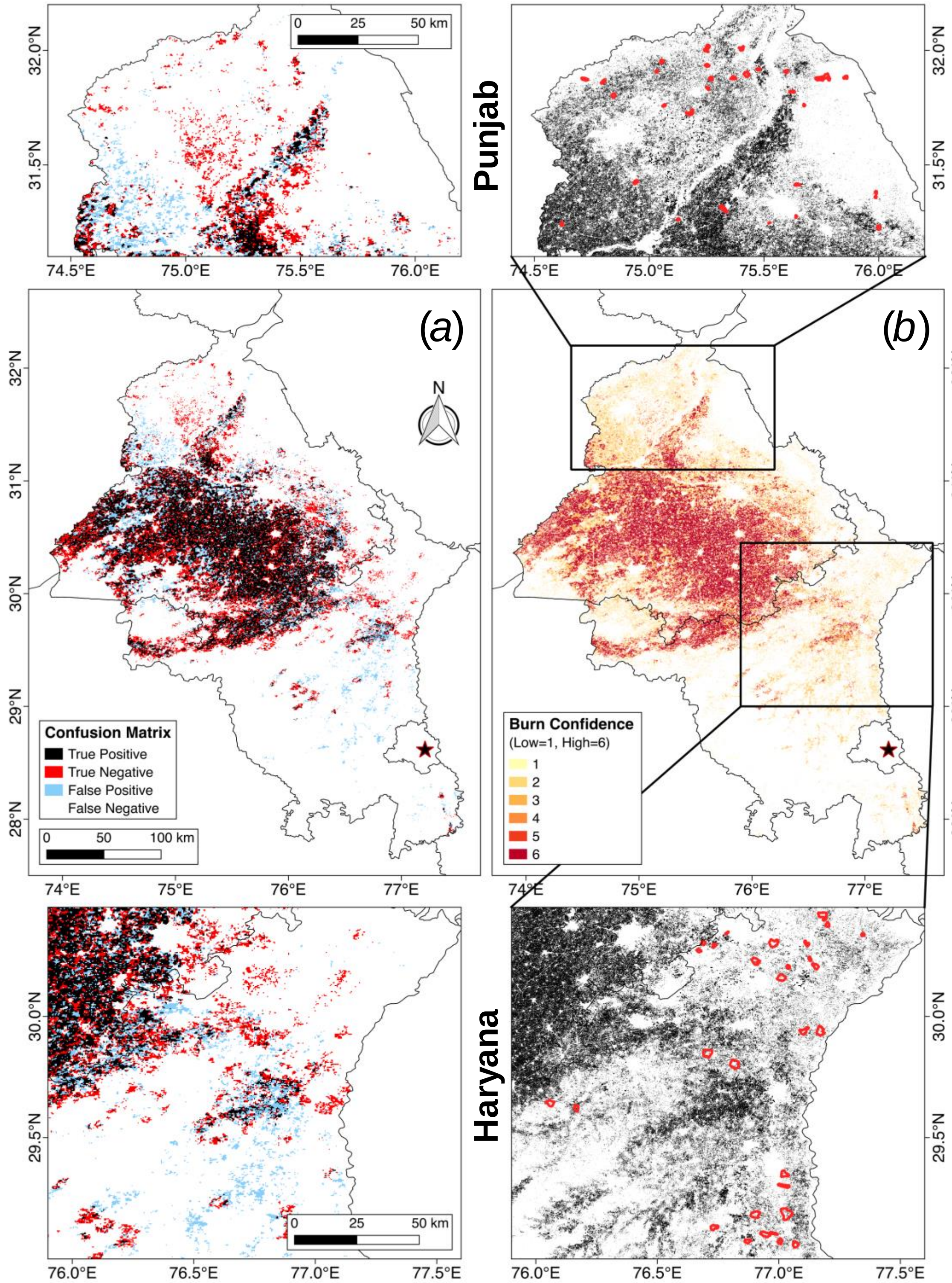


**Figure 7. ModL2T burned area classification**: (*a*) Agreement between $BA_{MCD64A1}$ and MODIS-only $BA_{ModL2T}$ and (*b*) classification confidence (Low = 1, High = 6) for $BA_{ModL2T}$ in Haryana and Punjab, post-monsoon (October-November) in 2016. The zoomed-in images show $BA_{ModL2T}$ (black) and the locations of the villages (red polygons) in Punjab (top row) and Haryana (bottom row) surveyed in 2016 for validation. The star denotes the location of New Delhi.

**Table 1.** Geographical accuracy assessment of $BA_{MCD64A1}$ (reference) and MODIS-only $BA_{ModL2T}$, in Punjab and Haryana, post-monsoon (October-November) in 2016 ($\kappa$ = 0.53, moderate agreement)

| MODIS-only $BA_{ModL2T}$ | MCD64A1 | | Producer's Accuracy |
|---|---|---|---|
| | Burned | Unburned | |
| Burned | 67634 | 49511 | 0.58 |
| Unburned | 31482 | 362183 | 0.92 |
| User's Accuracy | 0.68 | 0.88 | 0.84 |

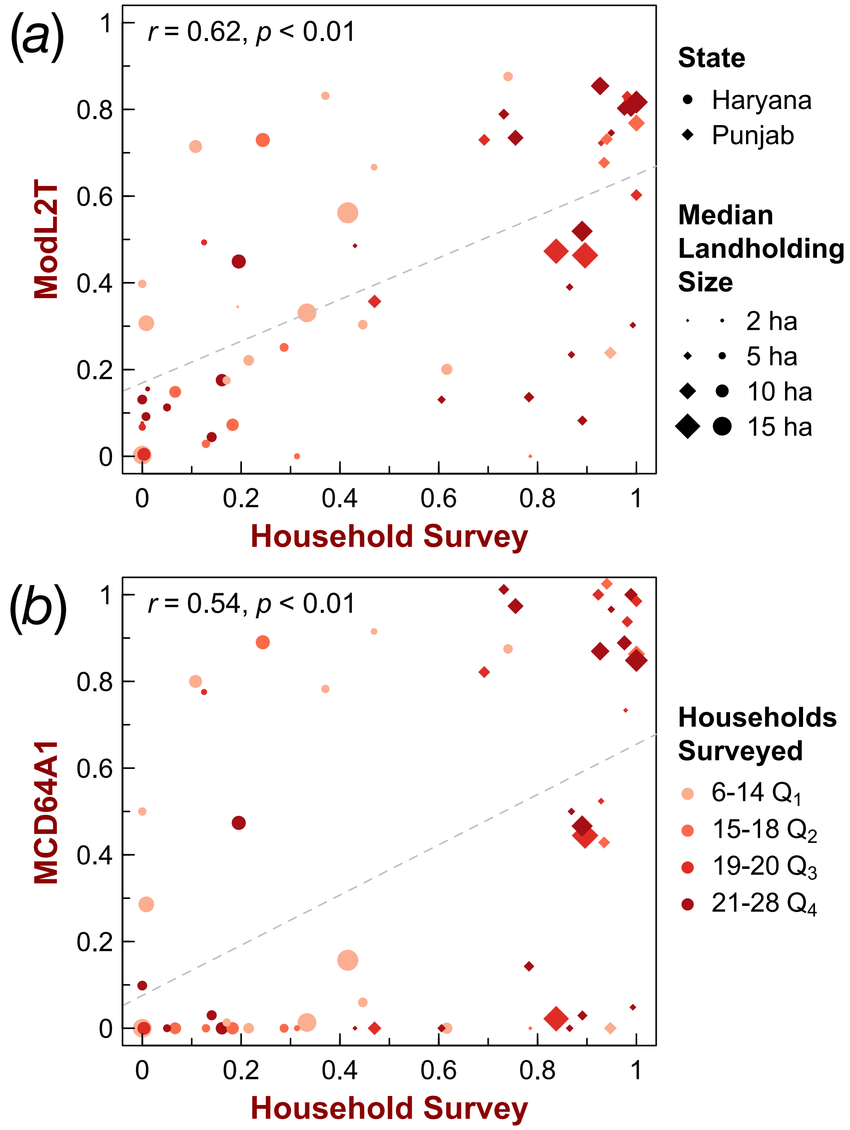


**Figure 8. Validation of satellite-derived burned area using household surveys**: comparison of % burning activity, normalized by landholding size, and % burned area from (*a*) ModL2T and (*b*) MCD64A1 in 30 Punjab (diamonds) and 32 Haryana (circles) villages during post-monsoon (October-November) in 2016. The size of the markers denotes the median landholding size, and the color denotes the quartile of the number of households surveyed.

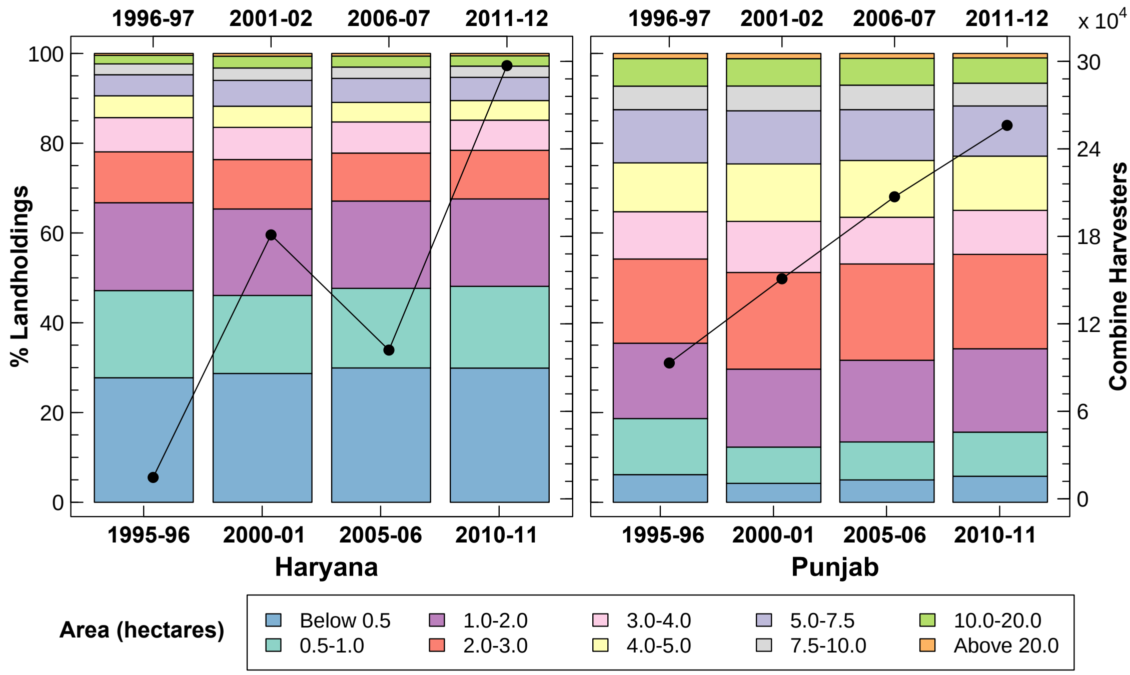


**Figure 9. Trends in landholdings by size and in use of combine harvesters in Punjab and Haryana**: Data from the Agricultural Census are in quinquennial intervals from 1995-96 to 2010-11 (landholdings) and the Input Survey, from 1996-97 to 2011-12 (combine harvesters).

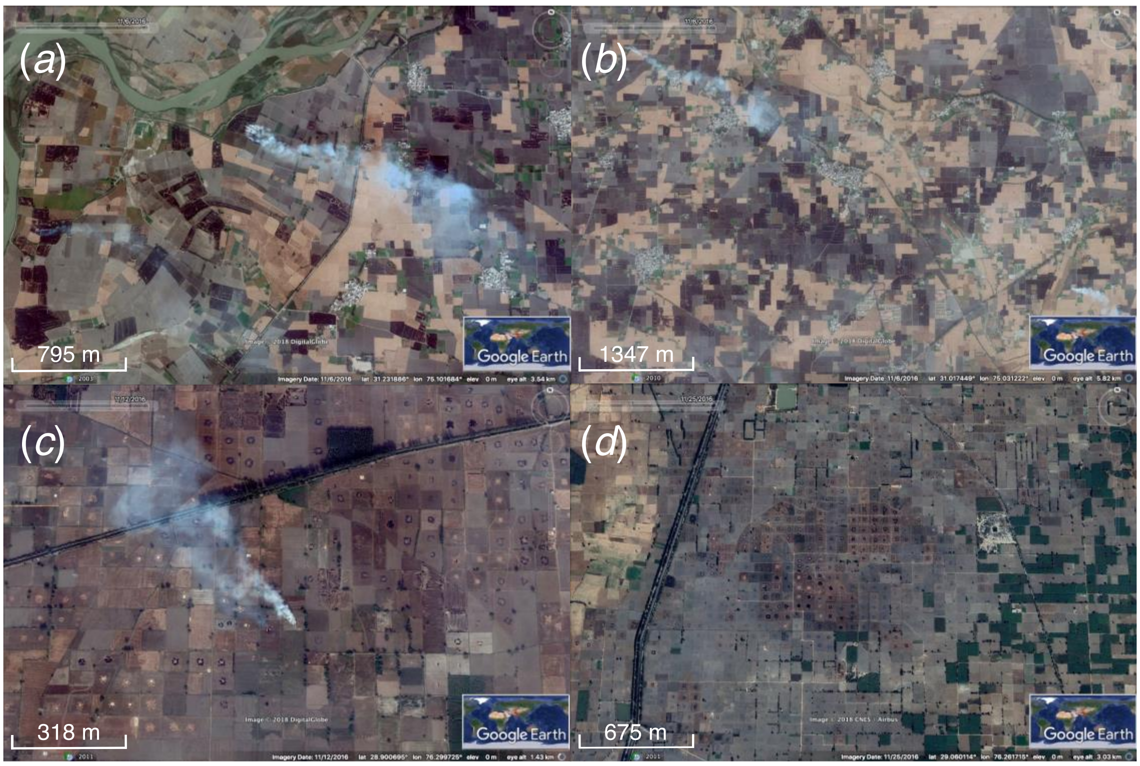


**Figure 10. Two crop residue burning practices**: Fine-resolution Google Earth DigitalGlobe and CNES/Airbus historical imagery of smoke and burn scars from crop residue burning in (*a* and *b*) central-northern Punjab (whole field) and (*c* and *d*) central Haryana (primarily partial field) in November 2016.